Climate Dynamics (1996) 12:325–357

Climate Dynamics

Intraseasonal oscillations in 15 atmospheric general circulation models: results from an AMIP diagnostic subproject

J. M. Slingo[1], K. R. Sperber[2], J. S. Boyle[2], J.-P. Ceron[3], M. Dix[4], B. Dugas[5], W. Ebisuzaki[6], J. Fyfe[7], D. Gregory[8], J.-F. Gueremy[3], J. Hack[9], A. Harzallah[10], P. Inness[8], A. Kitoh[11], W. K.-M. Lau[12], B. McAvaney[13], R. Madden[9], A. Matthews[1], T. N. Palmer[14], C.-K. Park[15], D. Randall[16], N. Renno[17]

[1] Department of Meteorology, University of Reading, 2 Earley Gate, Whiteknights, Reading, RG6 6AU, United Kingdom
[2] Program for Climate Model Diagnosis and Intercomparison, Lawrence Livermore National Laboratory, P.O. Box 808, L-264, Livermore, CA 94551, USA
[3] Meteo-France – Ecole Nationale de la Meteorologie, 42 Avenue G. Coriolis, F31057, Toulouse Cedex, France
[4] Division of Atmospheric Research, CSIRO, Private Bag No. 1, Mordialoc, Victoria 3195, Australia
[5] Recherche en Prevision Numerique, 2121 Trans-Canada Highway 500, Dorval, Quebec H9P 1J3, Canada
[6] NMC/NOAA, World Weather Building, Auth Road, Camp Springs, ND 20746, USA
[7] Canadian Climate Centre, University of Victoria, P.O. Box 1700 MS 3339, Victoria, BC V8W 2Y2, Canada
[8] Hadley Centre for Climate Prediction and Research, UK Meteorological Office, London Road, Bracknell, Berkshire RG12 2SY, United Kingdom
[9] National Center for Atmospheric Research, P.O. Box 3000, Boulder, CO 80307, USA
[10] Laboratoire de Meteorologie Dynamique de CNRS, Ecole Normale Superieure, 24, rue Lhomond 75231, Paris, Cedex 05 France
[11] Meteorological Research Institute, Nagamine 1-1, Tsukuba, Ibaraki 305, Japan
[12] Goddard Space Flight Center/NASA, Code 913, Greenbelt, MD 20771, USA
[13] Bureau of Meteorological Research Centre, GPO Box 1289K, Melbourne, Victoria 3001, Australia
[14] European Centre for Medium-Range Weather Forecasts, Shinfield Park, Reading, Berkshire RG2 9AX, United Kingdom
[15] Data Assimilation Office, NASA Goddard Space Flight Center, Code 910.3, Greenbelt, MD 20771, USA
[16] Department of Atmospheric Sciences, Colorado State University, Fort Collins, CO 80523, USA
[17] Mail code 170-25, Planetary Sciences, California Institute of Technology, Pasadena, CA 91125

Received: 9 February 1995 / Accepted: 17 August 1995

Abstract. The ability of 15 atmospheric general circulation models (AGCM) to simulate the tropical intraseasonal oscillation has been studied as part of the Atmospheric Model Intercomparison Project (AMIP). Time series of the daily upper tropospheric velocity poential and zonal wind, averaged over the equatorial belt, were provided from each AGCM simulation. These data were analyzed using a variety of techniques such as time filtering and space-time spectral analysis to identify eastward and westward moving waves. The results have been compared with an identical assessment of the European Centre for Medium-range Weather Forecasts (ECMWF) analyses for the period 1982–1991. The models display a wide range of skill in simulating the intraseasonal oscillation. Most models show evidence of an eastward propagating anomaly in the velocity potential field, although in some models there is a greater tendency for a standing oscillation, and in one or two the field is rather chaotic with no preferred direction of propagation. Where a model has a clear eastward propagating signal, typical periodicities seem quite reasonable although there is a tendency for the models to simulate shorter periods than in the ECMWF analyses, where it is near 50 days. The results of the space-time spectral analysis have shown that no model has captured the dominance of the intraseasonal oscillation found in the analyses. Several models have peaks at intraseasonal time scales, but nearly all have relatively more power at higher frequencies (<30 days) than the analyses. Most models underestimate the strength of the intraseasonal variability. The observed intraseasonal oscillation shows a marked seasonality in its occurrence with greatest activity during northern winter and spring. Most models failed to capture this seasonality. The interannual variability in the activity of the intraseasonal oscillation has also been assessed, although the AMIP decade is too short to provide any conclusive results. There is a suggestion that the observed oscillation was suppressed during the strong El Niño of 1982/83, and this relationship has also been reproduced by some models. The relationship between a model's intraseasonal activity, its seasonal cycle and characteristics of its basic climate has been examined. It is clear that those models with weak intraseasonal activity tend also to have a weak seasonal cycle. It is becoming increasingly evident that an accurate description of the basic climate may be a prerequisite for producing a realistic intraseasonal oscillation. In particular, models with the most realistic intrasea-

Correspondence to: J. Slingo

sonal oscillations appear to have precipitation distributions which are better correlated with warm sea surface temperatures. These models predominantly employ convective parameterizations which are closed on buoyancy rather than moisture convergence.

1 Introduction

The Atmospheric Model Intercomparison Project (AMIP) is a coordinated international effort to study simulations of the 1979–88 decade by all available current atmospheric general circulation models (Gates 1992). All the simulations employed the same sea surface temperatures, sea ice, solar constant and CO_2 concentration, thus enabling intercomparison of models that have been integrated under standardized conditions. As part of AMIP, a number of diagnostic subprojects have been proposed to study specific phenomena in some depth (Gates 1992). This study describes the first results from the subproject entitled 'Variability in the Tropics: Synoptic to Intraseasonal Timescales'. Periodicities implied by synoptic to intraseasonal time scales cover anything from 2 days up to as long as 80 days. Typically, periodicities between 2 and 10 days are associated with synoptic, westward moving phenomena, such as easterly waves. Lower frequencies tend to be dominated by periodicities between 30 and 60 days. Such phenomena are characterized by eastward propagation and have been variously named, but will be referred to here as the intraseasonal oscillation.

There are a number of reasons why this subproject should cover both the synoptic and intraseasonal time scales. Since most periodicities in the tropics are convectively driven, a separation of the two frequencies would be purely artificial. Indeed, recent satellite observations and modelling studies (Lau et al. 1989; Lau et al. 1991) have suggested that the two phenomena may be closely related. In practical terms, the same data will be needed for both time scales. In addition, the intraseasonal oscillation and the El Niño/Southern Oscillation (ENSO) both show similar evolutionary characteristics with an eastwards propagation of convective anomalies and a corresponding response by the large scale circulation, as discussed in Section 4. This has led to the suggestion that a link with these longer time scales may exist also (e.g., Lau and Chan 1988), even though the two phenomena have very different periodicities.

A pilot study of the tropical variability in a high resolution version of the ECMWF model has already shown that a GCM may have considerable skill in simulating the observed distribution and periodicities of tropical disturbances (Slingo et al. 1992). However, this result may be dependent on the convective parameterization. A similar study with the UK Universities Global Atmospheric Modelling Programme (UGAMP) GCM, integrated at lower horizontal resolution, typical of that used in AMIP, has shown that the representation of organized tropical convection at synoptic to intraseasonal time scales was extremely sensitive to the convective parameterization (Slingo et al. 1994).

The aim of this subproject is to increase our understanding of the possible processes involved in the development, propagation and dissipation of synoptic waves and of the intraseasonal oscillation. This might be achieved by the intercomparison of these phenomena in a large number of models with diverse resolutions and physical parameterizations. A similar study by Park et al. (1990) of the intraseasonal oscillation in three models suggests that the insight such an intercomparison might provide could be considerable. Listed below are the primary questions which this subproject aims to address:

1. How well do current GCMs represent synoptic to intraseasonal variability in the tropics?
2. Can the behavior of the intraseasonal oscillation be related to the incidence of synoptic variability, and/or vice versa?
3. Can we identify characteristics of the convective parameterization, such as the vertical profile of the heating, the closure (e.g., moisture convergence), which might influence the existence of synoptic and intraseasonal variability?
4. What seasonal and interannual variability can we identify? How does it compare with reality? Can we learn something about the controlling factors from such a comparison?
5. How does the intraseasonal oscillation depend on aspects of a model's basic climate?

The initial research for this subproject has concentrated on a basic assessment of the performance of the participating models with respect to their representation of the intraseasonal oscillation. In simple terms, the intraseasonal oscillation can be described as a near-global scale, quasi-periodic, eastward moving disturbance in the surface pressure, tropospheric temperature and zonal winds over the equatorial belt. It was first identified by Madden and Julian (1972) in a study of upper-air data, and has since been widely observed both in satellite and ground based measurements. The substantial modulation of tropical convection by the intraseasonal oscillation is readily apparent in satellite data (e.g., Lau and Chan 1985; Murakami et al. 1986). The availability of numerical weather prediction (NWP) analyses has meant that the basic planetary scale structures associated with the various phases of the oscillation are now well documented (e.g., Knutson and Weickmann 1987; Rui and Wang 1990). Since the oscillation has such a large effect on the diabatic heating over the Indian and West Pacific Oceans, it is not surprising that it also manifests itself in the extratropics (e.g., Ferranti et al. 1990). An intriguing aspect of the oscillation is its sporadic appearance, which shows considerable interannual variability, and for which no reasonable explanation yet exists. The influence of El Niño, for example, on the oscillation's structure, propagation and frequency of occurrence is not known. The AMIP decade covers two El Niño events (Fig. 1) and their possible influence on the observed and simulated

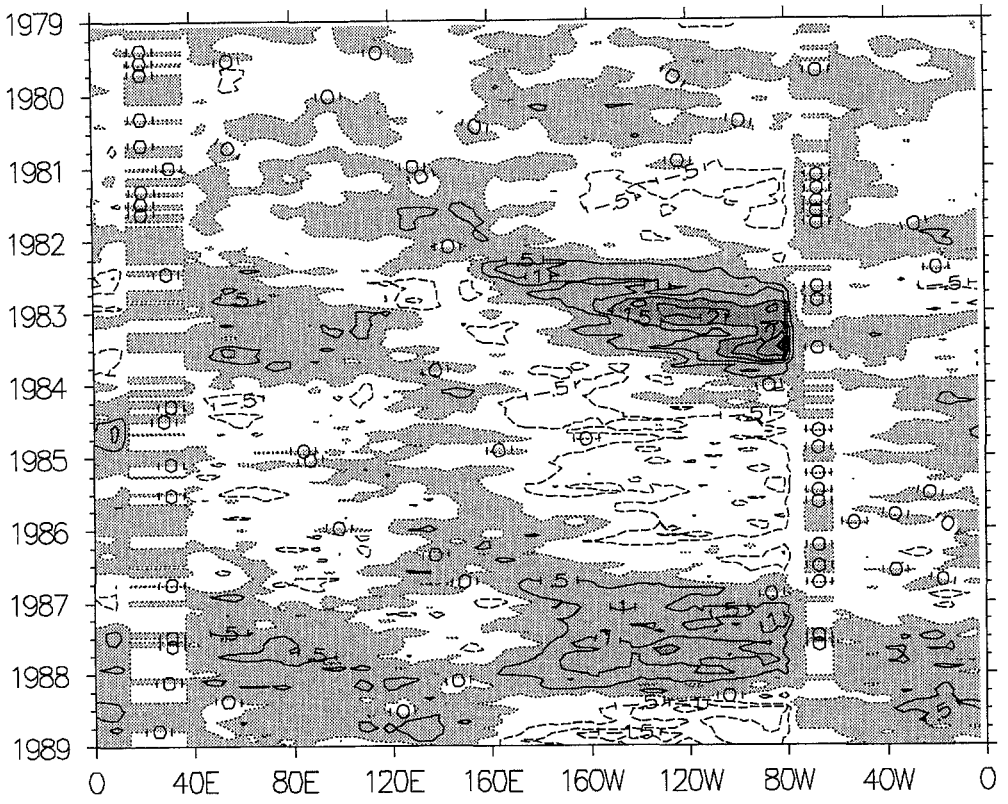

Fig. 1. Time-longitude diagram of the AMIP monthly mean sea surface temperature anomalies for the equatorial oceans, averaged between 10°N and 10°S. The contour interval is 0.5 K. Positive values are *shaded* and negative contours are *dashed*

intraseasonal oscillations will be considered in this study.

Despite the very important role that the intraseasonal oscillation plays in the tropical climate, its representation by GCMs has been problematic (e.g., Park et al. 1990). Although previous studies have shown that several models are capable of generating variability which possesses many of the characteristics of the observed oscillation (e.g., Slingo and Madden 1991; Hayashi and Golder 1993), there have remained some substantial deficiencies. In particular, the periodicity of the simulated oscillation tends to be too short, nearer 25–30 days than 40–50 days. The purpose of this study is to assess the current skill of GCMs in representing the intraseasonal oscillation and to identify possible factors that might offer scope for improvement in the future.

Since the acquisition and quality control of the complete AMIP history data is a lengthy process, those groups who had expressed interest in participating in the subproject were approached directly and asked to supply the following two fields:

Time series of daily 200 hPa velocity potential (χ), averaged between 10°N and 10°S.
Time series of daily 200 hPa zonal wind (u), averaged between 10°N and 10°S.

From these data a preliminary assessment of the simulated intraseasonal oscillation by each model was made. This paper will describe the results of this aspect of the subproject. More detailed analysis, possibly restricted to fewer models, will be the focus of subsequent research since a complete study of intraseasonal activity and any investigation of synoptic variability will require the full history of specific fields (e.g., winds, OLR).

Section 2 provides information on the participating models and the data used for validation, and Section 3, the basic methodology used to analyze the time series. Section 4 gives the background for the subsequent analysis; the results from each model, including aspects of their basic climatology, are presented in Section 5. Section 6 summarizes and discusses the results, and briefly presents plans for future work, including assessment of the synoptic variability.

2 Models and validation

The response by the participating modelling groups to the request for the time/longitude data described was very encouraging and 15 groups were able to send the necessary data. Table 1 shows the models and their acronyms whose results will be presented in this study. Note that CCC were only able to supply data at 300 hPa. Since the amplitude of the intraseasonal oscillation is observed to be greatest near 150 hPa (Slingo and Madden 1991; their Fig. 11), then the amplitude in the CCC results is likely to be less than the other models whose results were diagnosed at 200 hPa.

Two realizations were analyzed with the ECMWF model, based on different initial conditions but otherwise integrated with the same code. Included in Table 1 are some of the basic characteristics of the participat-

Table 1. List of models that participated in this study

Model	Resolution	Deep/shallow convection	Comments relevant to subproject
Bureau of Meteorology Research Centre (BMRC)	R31L9	Kuo/Tiedtke	
Canadian Climate Centre (CCC)	T32L10	Moist convective adjustment (MCA)	300 hPa data only, truncated at wave # 10
Centre National de Recherches Météorologiques (CNRM)	T42L30	Bougeault (moisture convergence closure)/Geleyn	'Emeraude' version
Commonwealth Scientific and Industrial Research Organisation (CSIRO)	R21L9	Moist convective adjustment (MCA)/Geleyn	
Colorado State University (CSU)	$4^0 \times 5^0$, L17	Arakawa-Schubert + MCA	
European Centre for Medium-range Weather Forecasts (ECMWF)	T42L19	Mass flux (Tiedtke; moisture convergence closure)	2 realizations
Goddard Laboratory for Atmospheres (GLA)	$4^0 \times 5^0$, L17	Arakawa-Schubert	
Goddard Space Flight Center (GSFC)	$4^0 \times 5^0$, L20	Relaxed Arakawa-Schubert	
Laboratoire de Météorologie Dynamique (LMD)	50 sinlat × 64 lon, L11	Kuo + MCA	
Meteorological Research Institute (MRI)	$4^0 \times 5^0$, L15	Arakawa-Schubert	
National Center for Atmospheric Research (NCAR)	T42L18	Mass flux (Hack)	
National Meteorological Center (NMC)	T40L18	Kuo/Tiedtke	
Recherche en Prévision Numérique (RPN)	T63L23	Kuo	Data truncated to T32
UK Universities Global Atmospheric Modelling Programme (UGAMP)	T42L19	Betts/Miller time lagged convective adjustment	
United Kingdom Meteorological Office (UKMO)	$2.5^0 \times 3.75^0$, L17	Mass flux (Gregory)	

ing models. Fuller details on the formulation of each model are available in Phillips (1994). In assessing the preliminary results, the basic climatology of each model has also been considered by making use of the AMIP standard output which has been prepared and quality controlled at the Program for Climate Model Diagnosis and Intercomparison (PCMDI).

Verification is an essential part of this subproject. Various datasets are being acquired, such as NWP analyses and satellite observations of outgoing longwave radiation (OLR). It is anticipated that the reanalysis projects in progress at ECMWF and the National Meteorological Center (NMC) will be invaluable. In this report, data from the Joint Diagnostics Project (JDP; Hoskins et al. 1989) have been used to provide similar diagnostics to those obtained from the models. The JDP represents an extensive programme of research carried out at the Department of Meteorology, Reading University, as part of UGAMP, to investigate many aspects of the atmospheric global circulation using ECMWF analyses. As part of the JDP, time series of daily velocity potential and zonal wind at 150 hPa, averaged between 10°N and 10°S, have been compiled by Matthews (1994) from ECMWF analyses for the years 1982–1990. These data were archived on a 5° grid and have been processed in the same way as the model results. The choice of level for the JDP was made prior to the design of the subproject, and the use of 150 hPa probably means that the amplitude of the oscillation in the JDP may be slightly larger than at 200 hPa. However, 200 hPa was chosen for the models as being more representative of outflow levels for cumulus convection for a range of convective parameterizations.

3 Methodology

The intraseasonal oscillation (IO) in the models and JDP data has been identified using the upper tropospheric velocity potential (χ), since the oscillation is seen most readily in this field, due to its planetary scale structure. The dynamical characteristics of the IO are elucidated further through evaluation of the upper tropospheric zonal wind (u), given the current paradigm that the IO consists of a Kelvin wave, modified by forced Rossby waves (e.g., Knutson and Weickmann 1987; Rui and Wang 1990; Hendon and Salby 1994). Since the seasonal cycle dominates the fields, the data for χ and u have been seasonally detrended. This was achieved by creating the 10-year mean for each day of the annual cycle and then computing the annual mean and first two harmonics from this time series. This mean and first two harmonics were then removed from the complete time series.

Each model has differing degrees of high frequency variability and intraseasonal time scales are not always readily apparent from the complete time series. For this reason various time filters have been applied to the data for differing purpose, to isolate intraseasonal, seasonal and interannual variability. For intraseasonal time scales, a 20–100 day bandpass filter is used; for seasonal and interannual time scales, a low pass filter with a 100 days cutoff is applied. Both are 100 point Lanczos filters; Fig. 2 shows the response curves for both filters.

A variety of spectral analysis techniques have been applied to the data to identify the dominant intraseasonal periodicities. Following Slingo and Madden (1991), the spectrum of the mean (SOM) has been

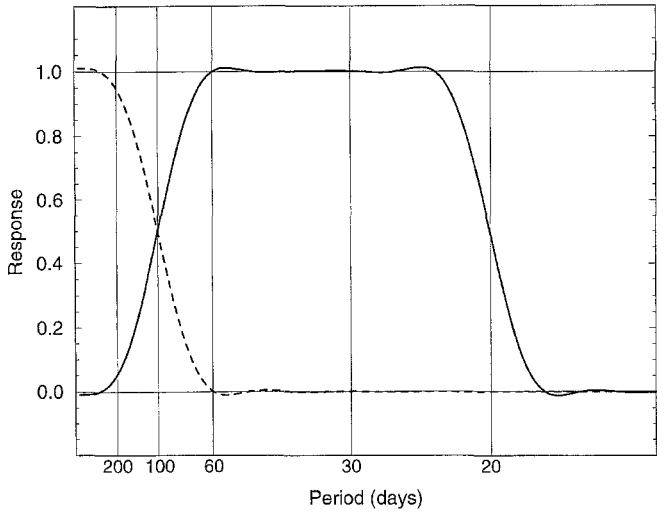

Fig. 2. Response curves of the low pass (>100 days) and band pass (20–100 days) filters used in this study

computed for area averages covering 45° in longitude. These SOMs have been found to be appropriate for identifying intraseasonal periodicities which have a planetary scale structure. The red noise spectrum was also calculated to give some idea of significant spectral peaks. Also following Slingo and Madden (1991), the dominant temporal and spatial scales of the disturbances have been determined through calculations of the cross-spectra and phase between pairs of time series from all possible combinations of longitude separations. Since the intraseasonal oscillation is observed to be an eastward moving phenomenon, space-time spectra have also been computed, following Hayashi (1982), in which the periodicities associated with eastward and westward travelling waves are identified separately. In this study only the results from the space-time spectral analysis will be shown, but these are entirely consistent with the results from the other spectral techniques applied to the data.

4 Background

To put the following discussion in context, and to support the approach used in the analysis of the model results, a résumé of the basic seasonal climate and the characteristics of the intraseasonal oscillation, as they might relate to that climate, will be given. Figure 3 shows the climatological upper tropospheric zonal wind for December, January, February (DJF) and June, July, August (JJA), based on ECMWF analyses. In the tropics, the zonal flow is predominantly easterly, but with some important seasonal variations, such as the stronger summer monsoon easterlies in the eastern hemisphere and the winter westerlies of the Pacific and Atlantic wave guides in the western hemisphere. These seasonal changes are sufficiently large that the zonal mean of the zonal wind for the equatorial belt (10°N–10°S) varies from mean westerlies in DJF to mean easterlies in JJA, thus contributing to the seasonal cycle observed in the total angular momentum and length of day (Rosen and Salstein 1983). A study of the intraseasonal, seasonal and interannual variation in the total angular momentum, as simulated by the participating models, is the topic of another AMIP diagnostic subproject (Gates 1992).

Also shown in Fig. 3 are the large scale divergent and rotational components of the upper tropospheric flow, as expressed by the velocity potential and the eddy streamfunction at 200 hPa. During the transition from DJF to JJA the main area of divergence moves off the equator with strong implied divergent (cross-gradient) flow westwards and southwards. The main implied polewards branch of the Hadley circulation moves from the Northern to the Southern Hemisphere. As shown from idealized model studies of the response of the rotational flow to equatorial heating (e.g., Sardeshmukh and Hoskins 1988), the eddy streamfunction shows the twin anticyclones near or to the west of the main centers of planetary scale divergent (i.e., heating) in the velocity potential. In DJF a strong pattern of Rossby waves is seen with twin cyclones forming to the east of the main area of equatorial heating. Much of the seasonal variation in the zonal wind can be related to the changes in the rotational flow in response to the diabatic heating.

The importance of the rotational flow in determining the response to an equatorial heating anomaly applies also to the El Niño/Southern Oscillation (ENSO) and to the intraseasonal oscillation. During an El Niño, the heating in the central and East Pacific increases; the winter upper tropospheric equatorial westerlies are weakened or disrupted and the zonal mean wind tends to easterly rather than westerly. Although some of the change in the zonal wind pattern can be attributed to the eastwards displacement of the main area of divergence, substantial changes in the pattern of the forced Rossby waves occur. The twin anticyclones move eastwards with the heating and the twin cyclones are disrupted. As with the seasonal cycle, these changes in the large scale circulation are reflected in interannual variations in the angular momentum and length of day. However the strength and pattern of these forced Rossby waves are sensitive to the basic state in which the anomalous heating exists. This can be seen in Fig. 4, where typical streamfunction difference patterns from ECMWF analyses for the warm (1987) versus cold (1988,89) phases of ENSO are shown for northern winter (January, February, March: JFM) and summer (JJA), following Rasmusson and Mo (1993). The heating anomalies associated with ENSO can be inferred from the outgoing longwave radiation (OLR) derived from measurements by the advanced very high resolution radiometer (AVHRR). These are also shown in Fig. 4 together with the response by the divergent part of the flow, implied by the upper tropospheric velocity potential. Although the anomalous heating pattern is similar in both JFM and JJA, the response of the rotational flow is very different and is much weaker during northern summer. It is important to appreciate this

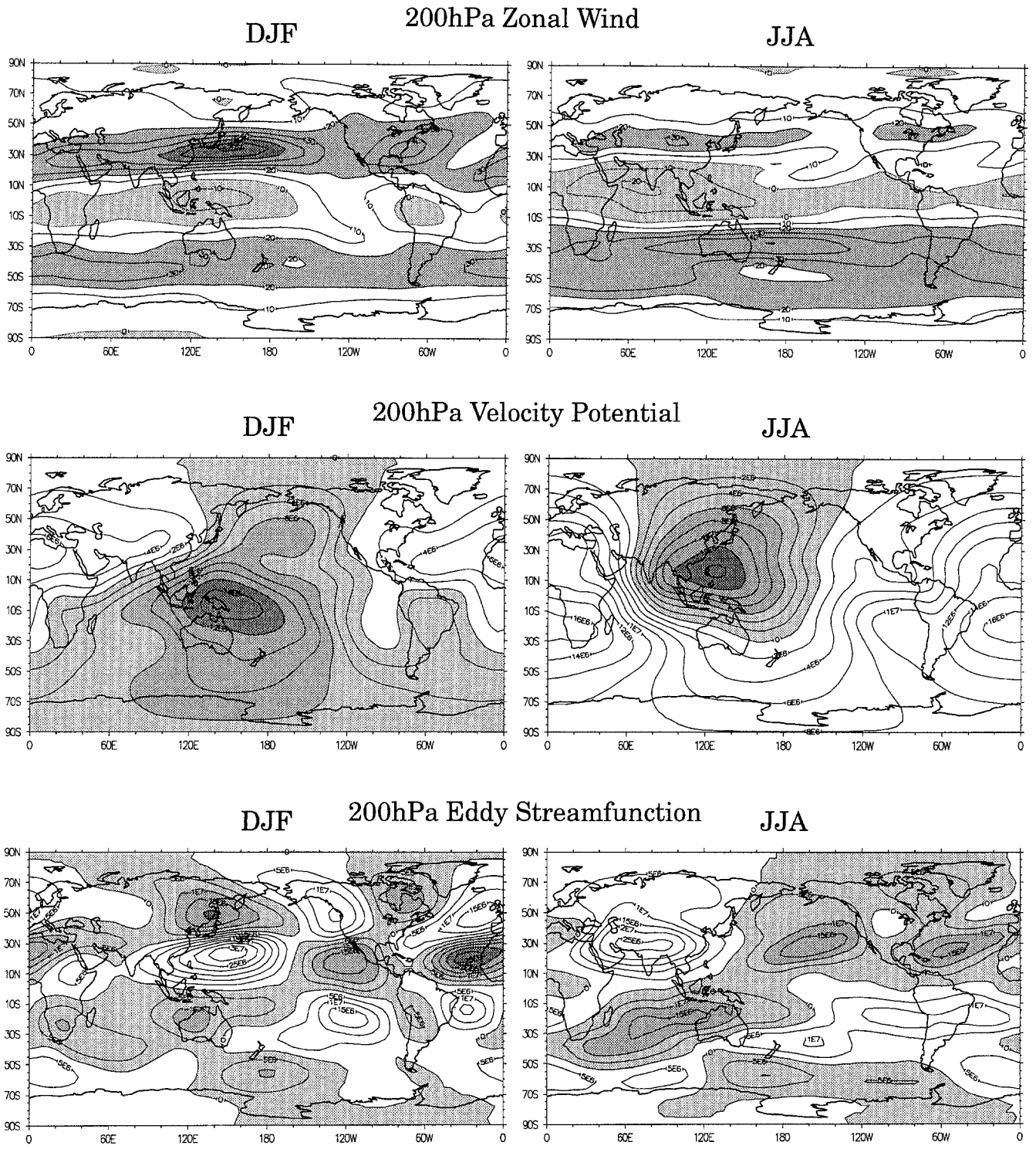

Fig. 3. Climatologies for DJF and JJA of zonal wind (u), velocity potential (χ) and eddy (asymmetric) streamfunction (ψ^*) at 200 hPa, from ECMWF analyses. The contour interval is 10 ms^{-1} for u, 2×10^6 $m^2\,s^{-1}$ for χ, and 5×10^6 $m^2\,s^{-1}$ for ψ^*. Easterlies, and westerlies in excess of 20 ms^{-1}, are *shaded* in u. Negative values of χ and ψ^* are *shaded*

seasonality in the Rossby wave response to equatorial heating anomalies.

At intraseasonal time scales, a substantial modulation of the diabatic heating occurs over the Indian Ocean and West Pacific. As noted by several authors (e.g., Knutson and Weickmann 1987; Rui and Wang 1990), the active (i.e., heating phase) of the IO over the eastern hemisphere produces a forced Rossby wave response as well as changes in the divergent component of the flow. Figure 5 shows the first EOF of the 150 hPa velocity potential and eddy streamfunction for DJF and JJA computed from ECMWF analyses which have been filtered to isolate intraseasonal time scales (Matthews 1994). The first EOF shows the dominant

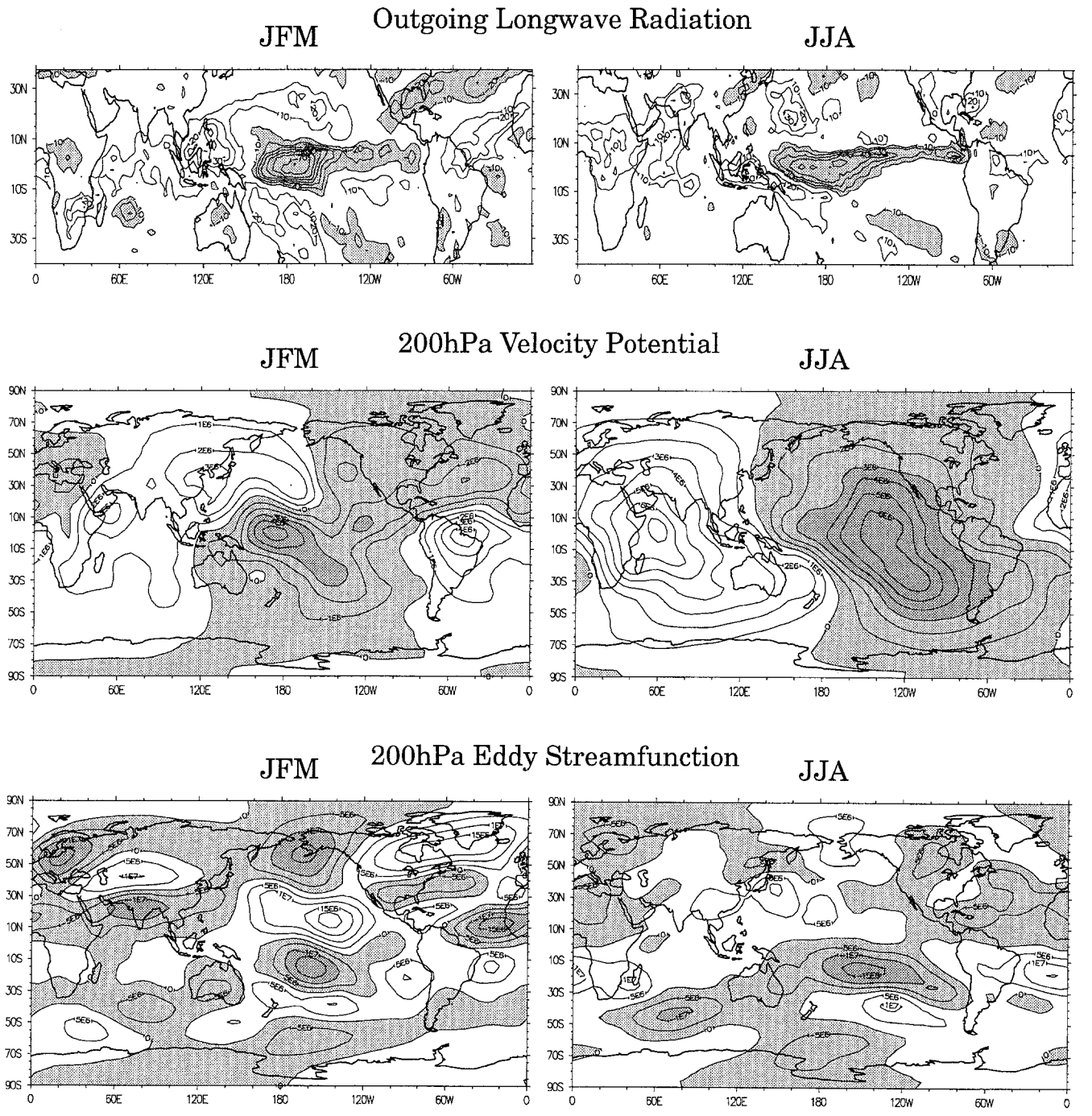

Fig. 4. Outgoing longwave radiation (OLR), velocity potential (χ) and eddy streamfunction (ψ^*) differences between El Niño and La Niña years, for northern winter (January, February, March, 1987 minus 1989), and northern summer (June, July, August, 1987 minus 1988). The contour interval is 10 Wm^{-2} (no zero contour) for OLR, 1×10^6 m^2 s^{-1} for χ, and 5×10^6 m^2 s^{-1} for ψ^*. Negative values of OLR, χ, and ψ^* are *shaded*

circulation anomalies produced when the active phase of the intraseasonal oscillation is located over the eastern Indian Ocean and maritime continent. The main heating anomaly is coincident with the increased planetary scale divergence, and as already noted both in the seasonal circulation patterns and the response to ENSO, twin anticyclones form near or to the west of the heating anomaly, with twin cyclones to the east, the phase difference being about 90°. These patterns are much more pronounced during DJF than in JJA, partly because the heating anomaly also tends to be stronger in DJF. The importance of the rotational flow response to the anomalous heating has led to the basic description of the IO as a circulation that involves both Kelvin and Rossby wave structures in the eastern hemisphere, where there are convective heating anomalies. In the western hemisphere, the upper tropospheric Kelvin wave alone is left which radiates away from the convective heating anomaly in the eastern hemisphere (e.g., Hendon and Salby 1994). This separate behavior

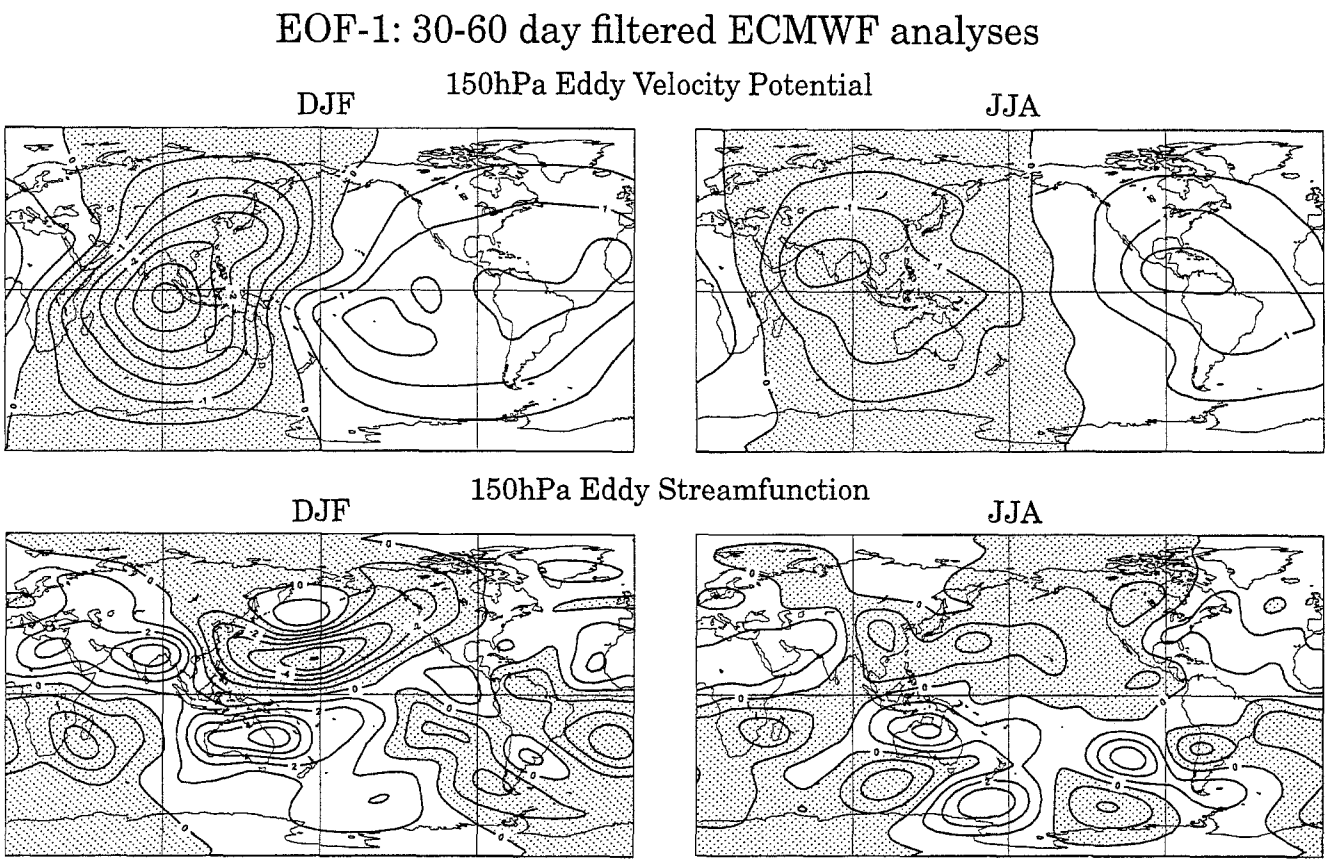

Fig. 5. The first EOFs of the 30–60 day filtered eddy velocity potential (χ^*) and eddy streamfunction (ψ^*) at 150 hPa for DJF and JJA based on ECMWF analyses. The contour interval is 0.5×10^6 $m^2\ s^{-1}$ for χ^*, and 1×10^6 $m^2\ s^{-1}$ for ψ^*. Negative values of χ^* and ψ^* are *shaded*

in each hemisphere is dependent on the convective instability and can be seen in the propagation speeds for the intraseasonal oscillation which tend to be faster in the western hemisphere, and nearer those expected for a dry Kelvin wave (Weickmann and Khalsa 1990).

The intraseasonal oscillation was first detected in the wind field (Madden and Julian 1972), and substantial wind anomalies exist in relation to the IO, as would be expected from the velocity potential and eddy streamfunction patterns seen in Fig. 5. As in the seasonal and interannual response to heating anomalies, these changes in the wind field are sufficiently large to be seen in the zonal mean wind. At intraseasonal time scales, modulation of the upper tropospheric zonal mean wind exceeds ± 2 ms^{-1}, with the transition between westerly and easterly being associated with the longitudinal position of the active phase of the oscillation. The modulation of the zonal mean wind by the intraseasonal oscillation arises primarily from the position of the forced Rossby modes with respect to the mean flow. The variations in the zonal wind translate into intraseasonal variability in the angular momentum and thence in the length of day (e.g., Magaña 1993), although the mechanisms by which this is achieved are still unclear (Madden and Julian 1994).

5 Results

5.1 Analysis of intraseasonal characteristics

The basic diagnostic for identifying the intraseasonal oscillation is the time-longitude diagram of velocity potential (χ), after seasonal detrending and temporal filtering with the 20–100 day filter. Figure 6 shows the time-longitude diagrams from the ECMWF analyses (hereafter referred to as JDP). The JDP results show a number of eastward moving disturbances which are sporadic in occurrence, but often make two or three apparent circuits of the equator. They are clearly more prevalent in northern winter and spring. Typical periodicities are between 40 days (e.g., early 1988) and 65 days (e.g., early 1985). The phase speed often appears to be faster over the western hemisphere, consistent with the results of Weickmann and Khalsa (1990). The apparent discontinuity in phase speed (e.g., early 1985) occurs near the dateline and represents a change in phase speed from near 6 ms^{-1} to 16 ms^{-1}. The latter is equivalent to a periodicity of just less than 30 days which is often the simulated periodicity of the intraseasonal oscillation in GCMs (e.g., Slingo and Madden 1991). The typical amplitude of the oscillation is $\pm 6 \times 10^6$ m^2/s^1, which represents a substantial modulation of the climatic mean χ field shown in Fig. 3. The

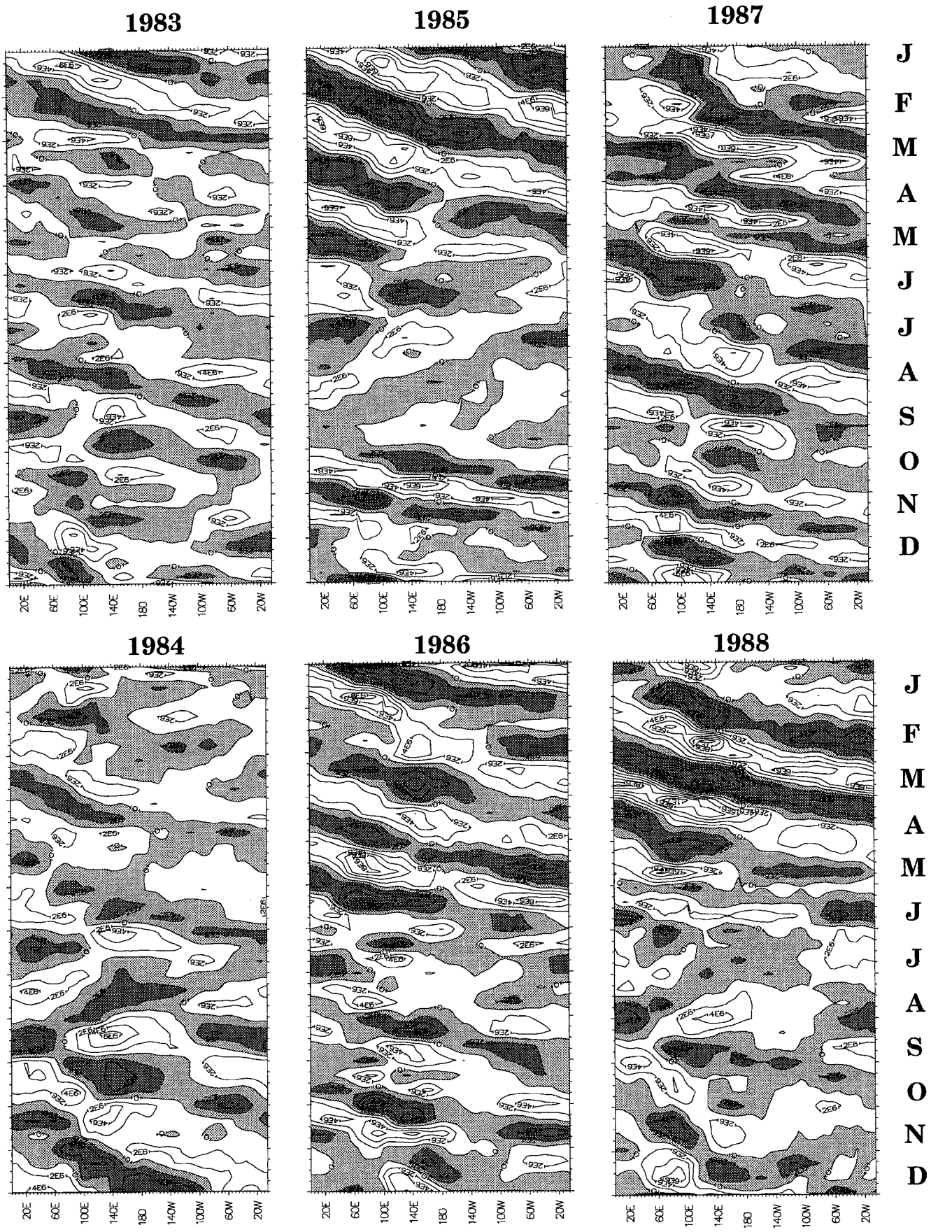

Fig. 6. Time-longitude diagrams of the 20–100 day filtered velocity potential at 150 hPa, averaged between 10°N and 10°S, from ECMWF analyses (JDP). The contour interval is 2×10^6 m^2 s^{-1} and negative values are *shaded*

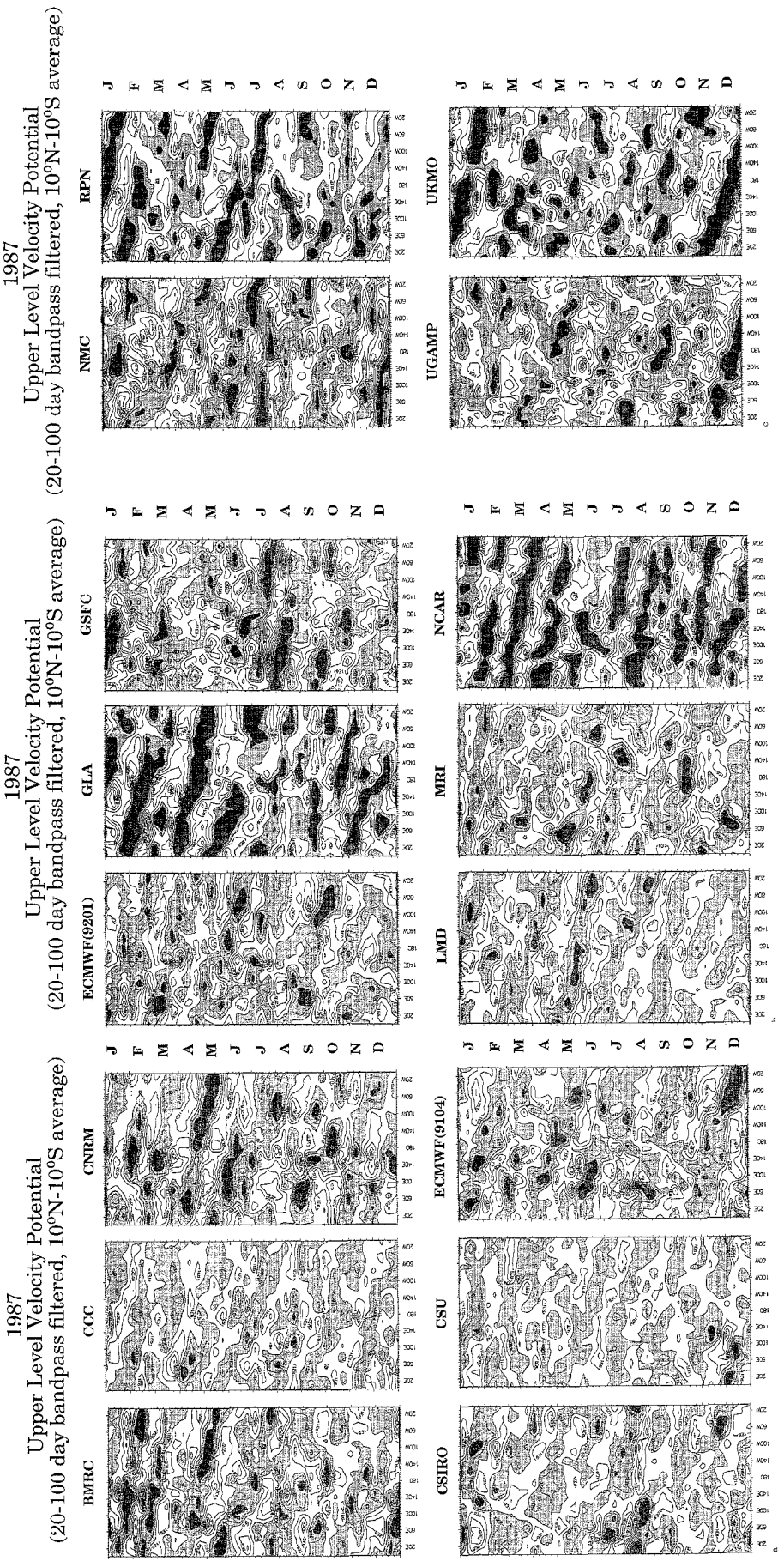

Fig. 7. Time-longitude diagrams for 1987 of the 20–100 day filtered velocity potential at 200 hPa (300 hPa for CCC), averaged between 10°N and 10°S, from the participating models. The contour interval is 1×10^6 m^2 s^{-1} for all models except GLA, NCAR, RPN and UKMO where it is 2×10^6 m^2 s^{-1}. Negative values are *shaded*

amplitude tends to be strongest in the eastern hemisphere where the convective activity is greatest.

The results from the participating models, including two realizations by the ECMWF model, are shown in Fig. 7. For brevity only the time-longitude diagrams for 1987 are given, but the behavior indicated by the results for that year is typical for each model. Fuller results are available in Slingo et al. (1995; WCRP). As Fig. 7 demonstrates, the models display a wide range of skill in simulating the intraseasonal oscillation. Note that the contour interval is half that used in the JDP, apart from the GLA, NCAR, RPN and UKMO results; thus the majority underestimate the strength of the intraseasonal variability. Most models show evidence of an eastward propagating anomaly although in some models there is a greater tendency for a standing oscillation, and in one or two the field is rather chaotic with no preferred direction of propagation. Where a model has a clear eastward propagating signal, typical periodicities seem quite reasonable although there is a tendency for the models to simulate shorter periods than in the JDP.

None of the model simulations of the IO show a systematic change in phase speed between eastern and western hemispheres, as observed in the JDP data. However, in several models there is a suggestion of two distinct disturbances with different phase speeds, one in which the disturbance propagates quite rapidly with speeds near 15 ms^{-1}, and another where the movement is much slower, near 6 or 7 ms^{-1}. There is also a suggestion in the JDP data of faster moving, but weaker, disturbances, for example in 1985 and 1987. Recently Hayashi and Golder (1993) identified two distinct disturbances, equivalent to periodicities of 50–60 days and 25–30 days in ECMWF analyses with the longer period being dominant, and noted that the GFDL model tended to prefer the faster moving (i.e., shorter period) waves.

When all the years are considered (Slingo et al. 1995; their Fig. 7), the clear seasonality of the intraseasonal oscillation in the JDP data is not seen in the model results, apart from GLA, RPN and UKMO in which the simulated amplitude is near that observed. Although NCAR has also simulated oscillations with a realistic amplitude, no preferred season is evident. Some models (e.g., CCC, CSIRO) appear to have more activity during northern summer and autumn. The two realizations with the ECMWF model have produced essentially the same result with regard to the amplitude and coherence of the simulated oscillation, but not with respect to the timing of each event, supporting the notion of an oscillation which is chaotic in nature. This result suggests that the basic ability of a GCM to simulate the intraseasonal oscillation can be identified from a single integration and does not depend on the initial conditions.

With all the models, the time-longitude diagrams are much less coherent than the JDP results, despite having been temporally filtered in the same way. The rather noisy character of the model results may be due to more activity at higher frequencies in the models than in the JDP data. The results of the space-time spectral analysis suggest that this is indeed the case. Since the intraseasonal oscillation is predominantly a wave-number one phenomenon (e.g., Slingo and Madden 1991), the complete space-time spectra are not shown. Instead the power spectra for the wave-number 1 of the χ field (seasonally detrended but otherwise unfiltered) have been computed for each year (June–May) of the data and the mean of the spectra calculated. The results are shown in Fig. 8. For convenience the frequencies corresponding to eastward travelling waves with periods of 70 and 30 days are highlighted. The JDP spectrum displays the dominance of the eastward travelling waves with preferred periodicities at intraseasonal time scales. It is clear from Fig. 8 that none of the models produce spectra which compare well with the JDP results. Several models have peaks at intraseasonal time scales, [e.g., CSIRO (40 days), GLA (60 days), RPN (30 days)], but nearly all have relatively more power at higher frequencies (<30 days) than the JDP. This is the case even for those models for which the χ time-longitude diagrams (Fig. 7) displayed a reasonable amplitude (i.e., GLA, NCAR, RPN, UKMO). Apart from these models, all the others underestimate the power associated with intraseasonal variability.

Whilst the velocity potential is a useful parameter for identifying the intraseasonal oscillation because of its planetary scale nature, the notion of eastward propagation, implied by such a field, can be misleading. Because it represents a potential, a negative anomaly at one location can arise purely from a positive anomaly at a remote location. The intraseasonal oscillation is considered to be an upper tropospheric Kelvin wave which propagates around the equatorial belt, with its structure modified by an associated forced Rossby wave in the eastern hemisphere. As a Kelvin wave, the oscillation should be identifiable as an anomalous zonal wind in the upper troposphere, with westerlies to the east of the divergence centre. This structure has been identified from radiosonde data (e.g., Madden and Julian 1972; Slingo and Madden 1991) and can be seen in the time-longitude diagram of the anomalous zonal wind (u) at 150 hPa from the JDP (Fig. 9a). The winds have been filtered with the same 20–100 day filter as used for the χ field. The agreement between the u and χ time-longitude diagrams is very good when the oscillation is strong, but note that for some occasions where a fully propagating signal is identified in χ (e.g., late 1985), no such signal exists in the u-wind. Again, the clear preference for the IO to occur during northern winter and spring is evident. The anomalies in u are substantial, reaching at least ± 6 ms^{-1} when the oscillation is strong (e.g., early 1985). As with χ, there appears to be a different character to the oscillation in the eastern hemisphere compared with the western hemisphere. East of the dateline the phase speed of the anomalies is much faster (e.g., 1988), and there is also a suggestion of a discontinuity in the propagation over the West Pacific (e.g., 1985).

The zonal wind time-longitude diagrams from the

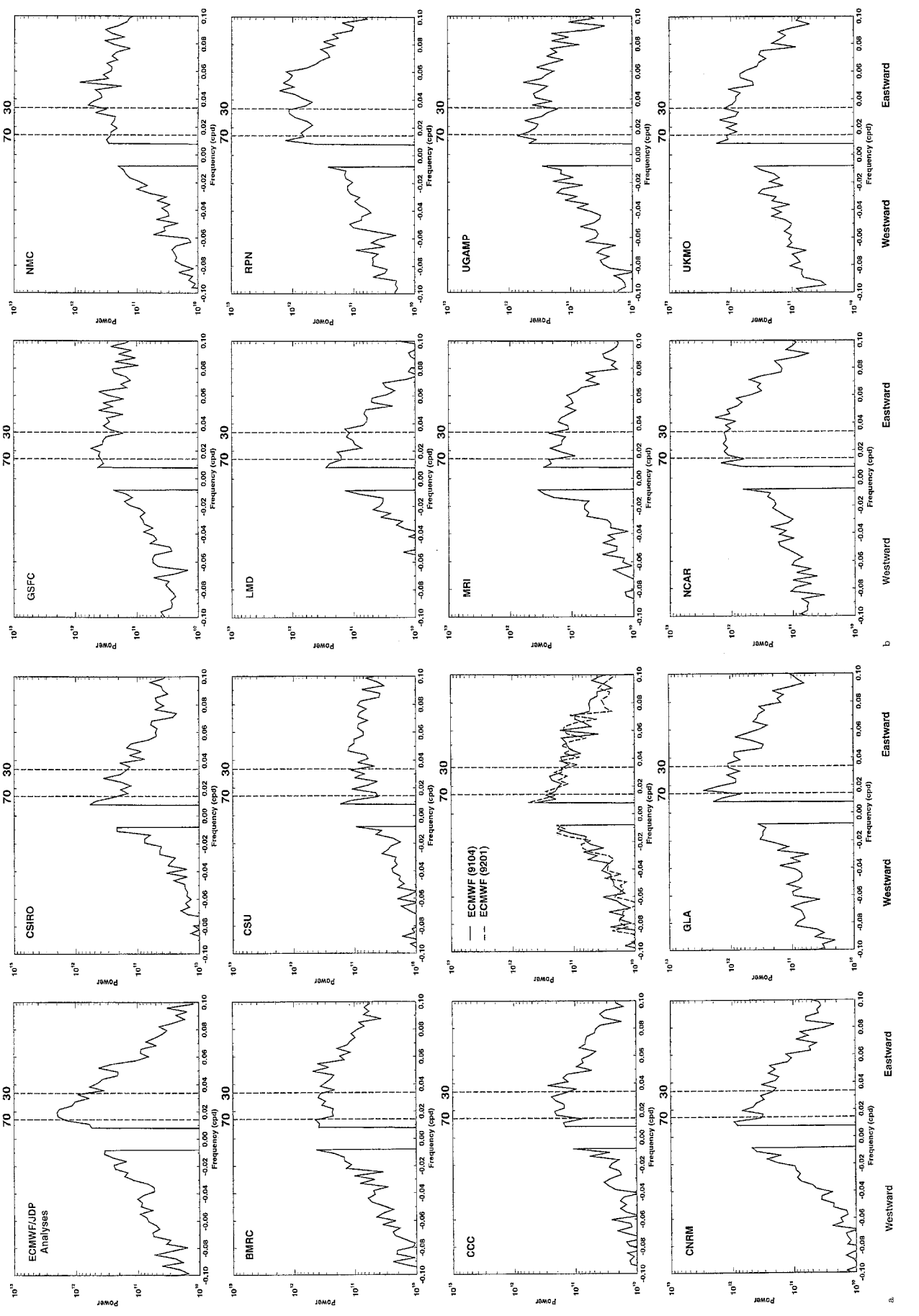
Upper Level Velocity Potential (10°N-10°S average)
Wave # 1 Power Spectra (June-May)
ECMWF/JDP Analyses
CSIRO
BMRC
CSU
CCC
ECMWF (9104)
ECMWF (9201)
CNRM
GLA
Upper Level Velocity Potential (10°N-10°S average)
Wave # 1 Power Spectra (June-May)
GSFC
NMC
LMD
RPN
MRI
UGAMP
NCAR
UKMO
Power
Frequency (cpd)
Westward
Eastward
a
b

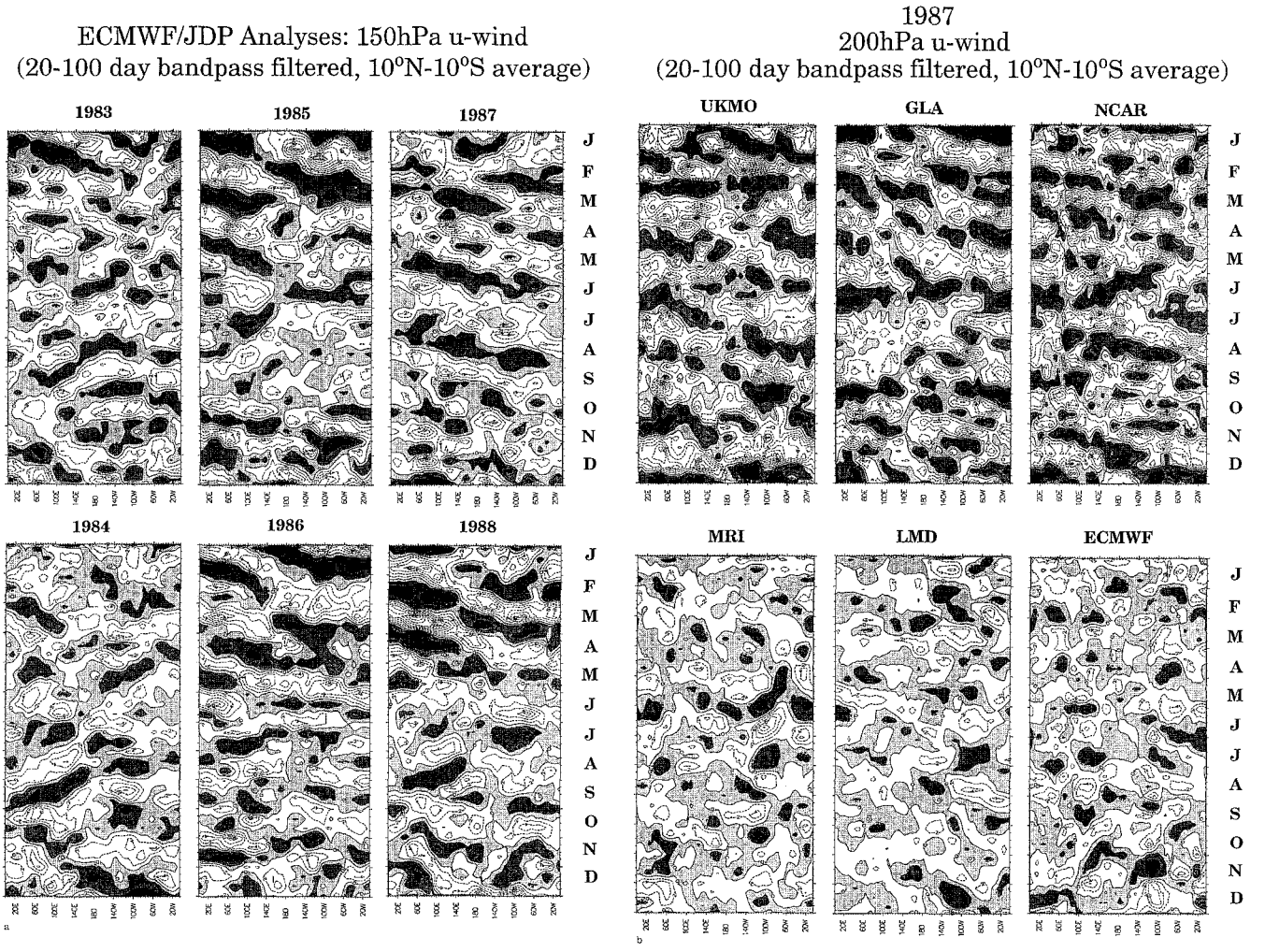

Fig. 9a, b. Time-longitude diagrams of the 20–100 day filtered zonal wind, averaged between 10°N and 10°S, from **a** ECMWF analyses (JDP) at 150 hPa, and **b** for 1987 from three models with a strong oscillation and three models with a weak oscillation. The contour interval is 2 ms^{-1}, and positive (westerly) values are *shaded*

models are very noisy, consistent with the results using χ. This can be seen in the examples of the zonal wind time-longitude diagrams for a single year, 1987, from three models with a strong intraseasonal oscillation and three with a weak oscillation in terms of χ (Fig. 9b). There is little evidence in any of the models of a coherent propagating signal in the u-wind, particularly over Indonesian and West Pacific longitudes. In fact the UKMO results show a discontinuity near the dateline and then some suggestion of an amplification of the oscillation in the East Pacific, perhaps associated with extratropical disturbances penetrating into the deep tropics in the Pacific waveguide (e.g., Kiladis and Weickmann 1992). In several instances these zonal wind anomalies propagate quite rapidly across the Greenwich Meridian, into the Indian Ocean. A similar behavior is also seen in the GLA results.

The space-time spectra for the JDP u-wind show that the spatial scale of the eastward moving waves is predominantly wave-number 1 but still with some power at wave-number 2. This result is consistent with the hypothesis that the intraseasonal oscillation consists of a wave-number 1 Kelvin wave modified by a wave-number 2 Rossby wave in the eastern hemisphere (e.g., Rui and Wang 1990). Since the power associated with wave-numbers greater than 2 is relatively small, only the spectra for wave-numbers 1 and 2 of the u-wind are shown in Fig. 10. Again, the JDP data have strong spectral peaks at intraseasonal time scales with the dominant periodicity near 50 days and a secondary peak near 30 days. This result is in general agreement with a similar diagnosis of ECMWF analyses by Hayashi and Golder (1993). However, their result suggests a slightly longer dominant period in excess of 50 days and little evidence of the shorter period near 30 days. It is noteworthy that their data cover a slightly different period (1979–87) than the JDP (1982–90) and that they comment on the considerable interannual varia-

Fig. 8. Space-time spectra for the eastward and westward moving waves of the wave-number 1 seasonally detrended velocity potential. The *dashed vertical lines* indicate periodicities of 70 and 30 days

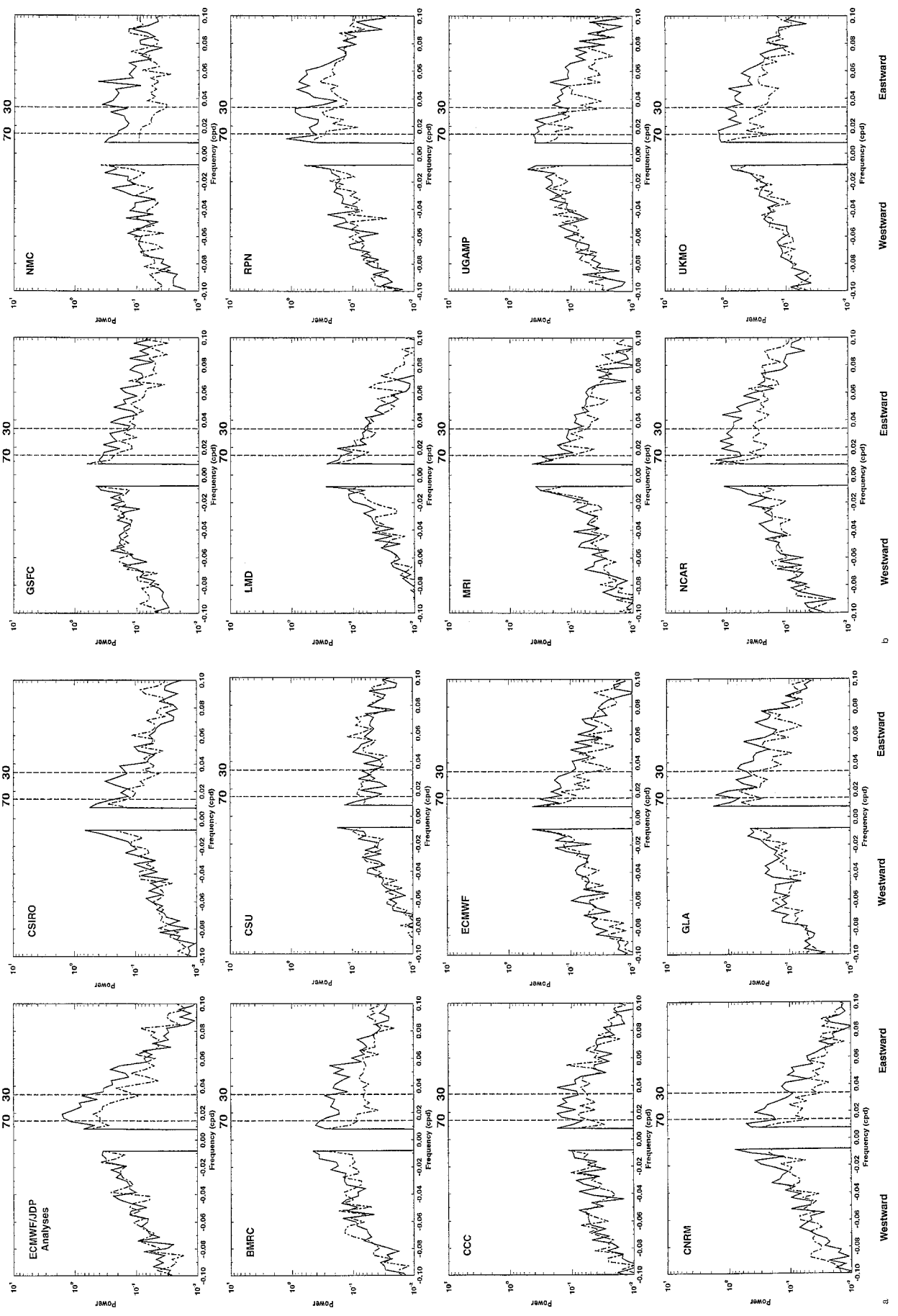
Upper Level u-wind (10°N-10°S average)
Wave # 1 and 2 Power Spectra (June-May)
ECMWF/JDP Analyses
CSIRO
BMRC
CSU
CCC
ECMWF
CNRM
GLA
GSFC
NMC
LMD
RPN
MRI
UGAMP
NCAR
UKMO
Power
Frequency (cpd)
Westward
Eastward
a
b

bility in the spectra. This variability in the period of the intraseasonal oscillation can also extend over a number of years as was noted by Slingo and Madden (1991) and Madden and Julian (1994).

As with χ, the model zonal wind spectra show poor correspondence with the JDP spectra both in terms of dominant periodicities and in the associated power (Fig. 10). The JDP spectrum has an actual peak in the 30–70 day time scale with the decreasing power at lower frequencies, whereas the models display approximately red noise spectra with increasing power at lower frequencies, all the way to the longest resolved time scales. Apart from GLA, NCAR, RPN and UKMO, the overall power simulated by the models is considerably less than in the JDP, but with relatively more at higher frequencies. None of the models have reproduced the dominant wave-number 1 intraseasonal periodicities of the JDP, and several models also have excessive power at intraseasonal time scales associated with westward moving waves (e.g., GSFC, UGAMP). Thus the noisy appearance of the time-longitude diagrams may also be associated with improper partitioning of the variance between eastward and westward moving waves. If the variance of the zonal wind is approximately equipartitioned between eastward and westward propagating modes, then the dominance of one or other is governed by their amplitude and relative phasing, possibly giving rise to the irregular structure of the time-longitude diagrams based on filtered data. The partitioning of power between wave-numbers 1 and 2 in the models is similar to the JDP results, suggesting that some aspects of the models' intraseasonal behavior may be consistent with the paradigm of a Kelvin wave modified by a forced Rossby wave. However, the generally poor agreement between the JDP and model spectra suggests that even when the intraseasonal oscillation is reasonably represented in terms of the χ time-longitude (Fig. 7), those models may be simulating intraseasonal activity whose characteristics do not resemble the observations.

The wide range of skill displayed by the various models is an interesting although not altogether a surprising result, bearing in mind previous problems in simulating the intraseasonal oscillation. It is disappointing that none of the models seem to simulate reasonable space-time spectra, since both the NCAR Community Climate Model (CCM1) run in perpetual January mode (Slingo and Madden 1991) and the GFDL model, run in seasonal cycle mode (Hayashi and Golder 1993) showed some skill in simulating various aspects of the observed oscillation. In the following sections some attempt will be made to relate a model's intraseasonal variability to its seasonal and interannual characteristics, as well as aspects of its basic climate, as given in the AMIP standard output. In this study the analysis has necessarily been limited by the lack of comprehensive history data and so as much as possible has been gleaned from the time-longitude datasets.

Fig. 10. Space-time spectra for the eastward and westward moving waves of the wave-numbers 1 (*solid*) and 2 (*dashed*) for the seasonally detrended zonal wind. The *dashed vertical lines* indicate periodicities of 70 and 30 days

5.2 *Relationship to seasonal variability*

In Section 4 the planetary scale response to changes in diabatic heating, whether they be interannual, seasonal or intraseasonal, was discussed, and the similarity of the tropical response was noted. Therefore, it may be useful to consider a model's intraseasonal variability in the context of its seasonal behavior. As already noted, the planetary scale response to diabatic heating gives systematic changes in the upper tropospheric zonal mean u-wind ($\bar{u}$), particularly at seasonal time scales. In Fig. 11 the evolution of $\bar{u}$, averaged between 10°N and 10°S, has been plotted for the JDP and, for brevity, from two participating models, which are representative examples of models with weak and strong oscillations. The seasonal and intraseasonal characteristics of the zonal wind have been identified by filtering the data with low pass (>100 days) and band pass (20–100 days) filters. Full results for all the participating models are given in Slingo et al. (1995).

The response of $\bar{u}$ to the seasonal cycle can be seen in the JDP data with the annual transition from mean westerlies in northern winter to mean easterlies in summer, associated with the Asian summer monsoon. A semi-annual modulation of the zonal wind is also evident, with the westerlies having two distinct maxima near mid winter and in late May, before the onset of the monsoon. Although the seasonal cycle dominates the evolution of $\bar{u}$, there is also substantial modulation at intraseasonal time scales. On some occasions, when the intraseasonal oscillation is particularly strong (e.g., 1988, see Fig. 6), the effect on $\bar{u}$ is sufficiently large to change the seasonal mean westerlies to strong easterlies.

The same diagnostics from the models again show a wide range of skill. Several models have an overall easterly bias, but, if that is taken into account, most show the seasonal transition from winter westerlies to summer easterlies, and the semi-annual behavior of the westerlies. Several models underestimate the amplitude of the seasonal cycle, an exception being the UKMO where it is overly strong (note change in scale). In general there is considerable interannual variability in $\bar{u}$, although one or two models (e.g., LMD and MRI) have simulated a very regular annual and semi-annual oscillation.

At intraseasonal time scales, the modulation of $\bar{u}$ simulated by the models is in general agreement with the relative strengths of the intraseasonal oscillations seen in Fig. 7. Those models with a very weak or ill-defined oscillation in terms of χ, are also those with weak modulation of the zonal mean u-wind. The results also suggest that strong intraseasonal variability is correlated with strong seasonal variability. Those models with a weak intraseasonal oscillation tend also to

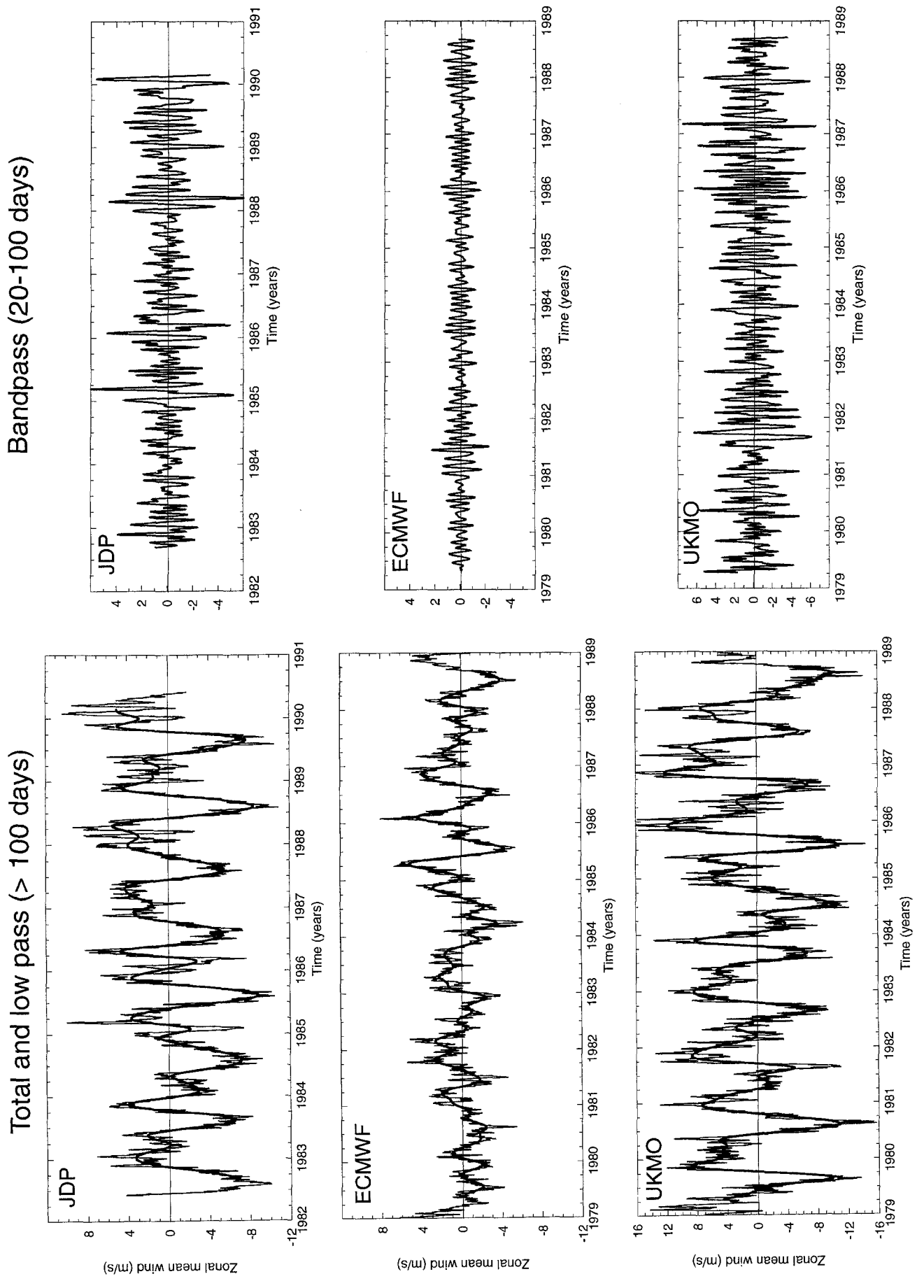
Total and low pass (> 100 days)
Bandpass (20-100 days)
JDP
ECMWF
UKMO
Zonal mean wind (m/s)
Time (years)

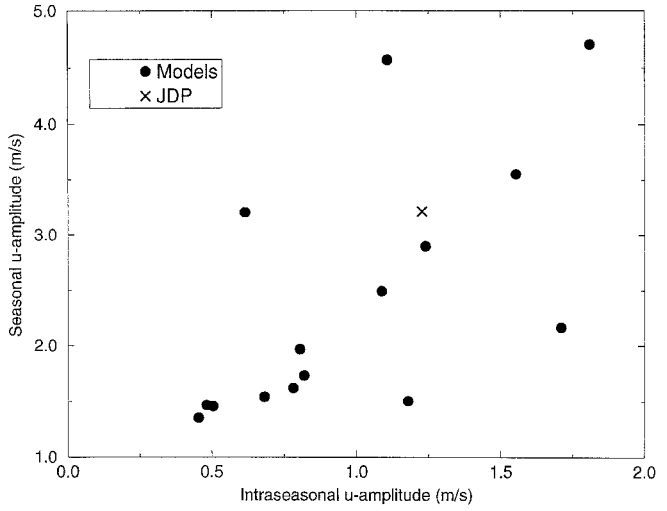

Fig. 12. Scatter plot of the mean amplitude of the seasonal cycle in the zonal mean u-wind versus the mean amplitude of the intraseasonal variations in the zonal mean u-wind

Table 2. Mean amplitude of the intraseasonal and seasonal variability in the zonal mean u-wind at 200 hPa from the participating models and from the ECMWF analyses (JDP)

Model (number)	20–100 days	>100 days
BMRC (9)	1.11	4.57
CCC (300 hPa)	0.68	1.54
CNRM (6)	0.80	1.97
CSIRO (5)	0.78	1.62
CSU (1)	0.45	1.35
ECMWF (2)	0.48	1.47
GLA (13)	1.71	2.17
GSFC (11)	1.24	2.90
LMD (3)	0.51	1.46
MRI (4)	0.62	3.21
NCAR (12)	1.55	3.55
NMC (7)	0.82	1.74
RPN (10)	1.18	1.51
UGAMP (8)	1.09	2.50
UKMO (14)	1.81	4.71
JDP (150 hPa)	1.23	3.21

have weak or poorly simulated seasonal variability. Conversely, those with a very strong seasonal cycle tend to have a strong oscillation. If the intraseasonal and seasonal activity of each model is quantified in terms of the mean amplitude of the bandpass and low-pass $\bar{u}$, respectively, then the relationship between them is shown in the scatter diagram given in Fig. 12. A positive correlation with a coefficient of 0.64 is evident between the seasonal and intraseasonal variability, suggesting that if the simulated strength of the seasonal cycle is improved in a model, then the intraseasonal variation may be also.

The mean amplitude of the bandpass filtered $\bar{u}$ appears to be a useful parameter for quantifying the intraseasonal activity in each model and in the JDP data. Its magnitude is consistent with the time-longitude diagrams shown in Fig. 7; it also represents a synthesis of how intraseasonal variability in the heating translates into modification of the planetary scale circulation patterns. In Table 2, the models are ranked in terms of their intraseasonal activity by using the mean amplitude of the bandpass filtered $\bar{u}$. The model number will be used later when various aspects of a model's formulation and performance are studied and related to that model's ability to simulate intraseasonal variability. Note that the CCC has not been numbered since the zonal wind was supplied at a different pressure level (300 hPa).

At the beginning of Section 4 it was argued that the seasonal evolution of the zonal wind field was related to the response of the planetary scale divergent and rotational flow to changes in the diabatic heating. If we consider that χ represents a reasonable indicator of changes in deep tropospheric heating, primarily associated with cumulus convection, then we can see that those models with strong modulation of the heating field at intraseasonal time scales are also models with a strong dynamical response in terms of the zonal wind field. There is a tendency for this to be the case at seasonal time scales also. In Fig. 13, the mean seasonal evolution of the equatorial (10°N–10°S) χ field is shown, based on the annual mean and first two harmonics of the 10 year mean daily time series. As noted in Section 3, this was used to detrend the data before analyzing intraseasonal variability. In the absence of any other data, this field provides a very basic description of the seasonal evolution of the large scale heating pattern in terms of its strength and longitudinal position. The JDP data show the shift westwards of the main area of heating and intensification of the upper level divergence associated with the Asian summer monsoon. The models again display a large range in skill with the seasonal evolution in the large scale heating, implied by χ, being highly variable between models. Not all show the westward movement of the heating in northern summer and some models have substantial errors in the pattern. Those models with a weak seasonal cycle in $\bar{u}$ tend also to have generally weak amplitude in their large scale heating patterns, implied by Fig. 13.

The inference from these results is that those models with a strong intraseasonal activity are also those whose diabatic heating processes respond strongly to the seasonal cycle. They probably represent models that have an active cumulus convection scheme which responds well to the forcing, be it seasonal, related to the insolation; interannual, related to ENSO; or other higher frequency perturbations such as the influence of the extratropics. They may also be models whose convection schemes produce more activity at synoptic fre-

Fig. 11. Time series of the upper tropospheric zonal mean u-winds from ECMWF analyses (JDP): total (*left panel, thin line*) and low pass filtered (>100 days; *left panel, thick line*), and band pass filtered (20–100 days; *right panel*). Data for two participating models, ECMWF and UKMO, are also given

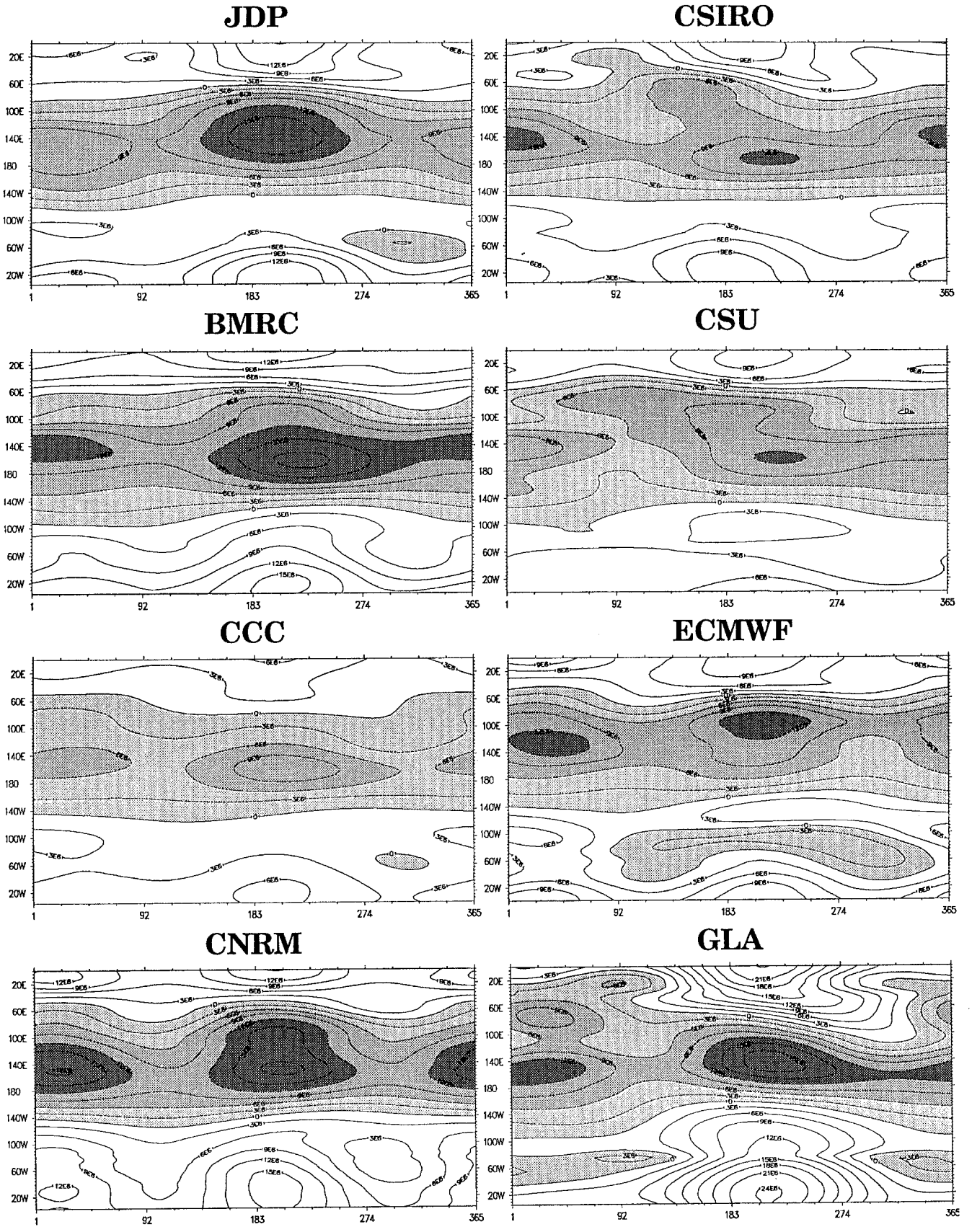

Fig. 13. Time-longitude diagrams of the mean and first two harmonics of the average annual cycle of the upper level velocity potentia from ECMWF analyses (JDP) and the participating models. The contour interval is 3×10^6 m^2 s^{-1} and negative values are *shaded*

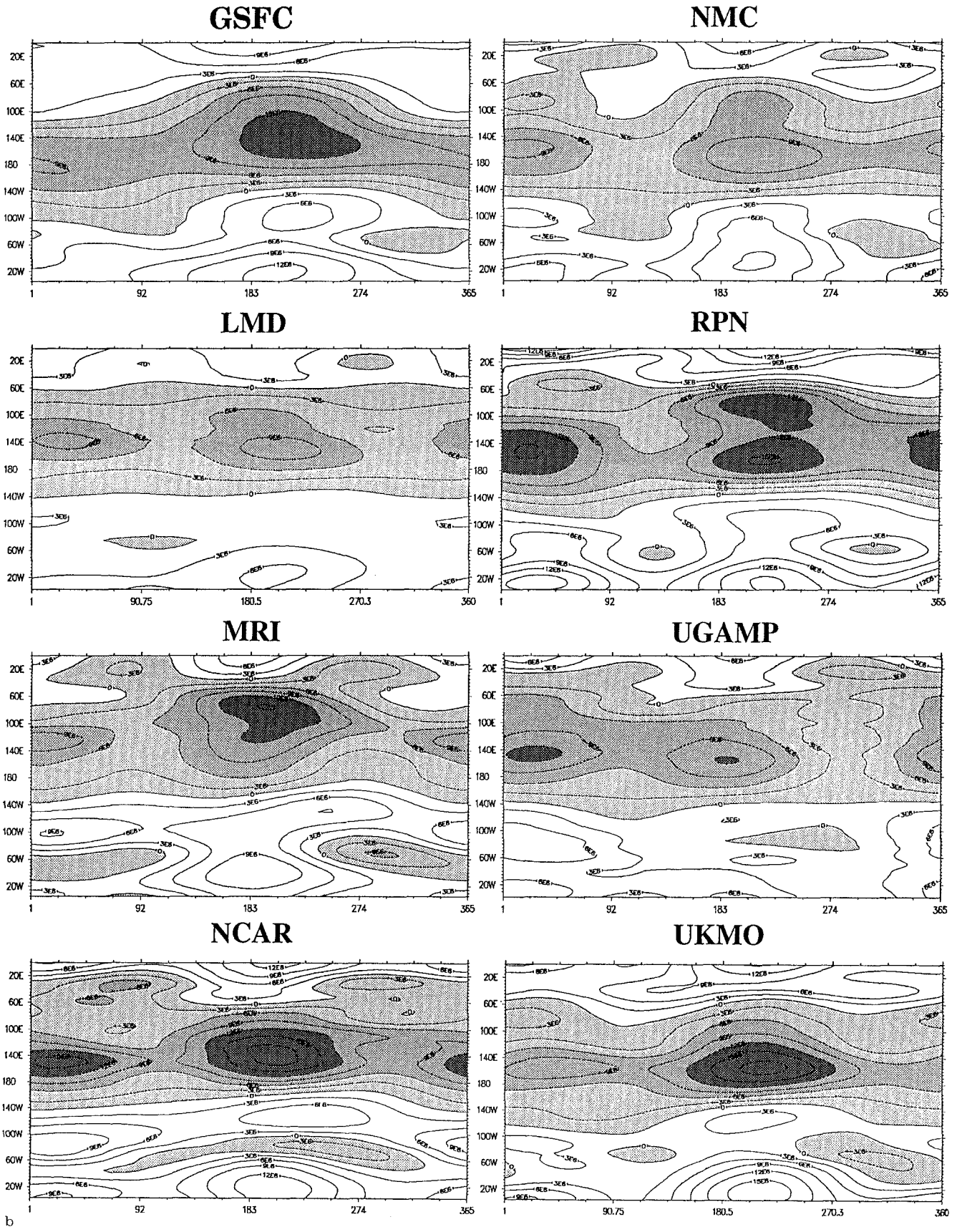
GSFC
NMC
LMD
RPN
MRI
UGAMP
NCAR
UKMO
20E
60E
100E
140E
180
140W
100W
60W
20W
1
92
183
274
365
90.75
180.5
270.3
360

b

quencies (<20 days). For example, results from a study of convective parameterization in the UGAMP model have shown that a convection scheme which gives more organization at synoptic scales also produces more realistic intraseasonal variability (Slingo et al. 1994). A recent study by Hendon and Liebmann (1994) of the organization of convection within the intraseasonal oscillation has shown that synoptic activity is substantially enhanced during the active phase of the oscillation. The realtionship between these two time scales will be investigated further in the next phase of research in this subproject when more detailed history data are available.

5.3 *Interannual variability and response to El Niño*

The sporadic appearance of the observed intraseasonal oscillation and its substantial interannual variability in intensity (e.g., Salby and Hendon 1994) have not been adequately explained. The possibility that the oscillation might be sensitive to the phase of El Niño has not been addressed, apart from the suggestion by Gray (1988) and Kuhnel (1989) that the oscillation tends to have a higher frequency during El Niño. With regard to the level of activity of the oscillation, the results of Salby and Hendon (1994) and Hendon and Liebmann (1994) suggest that any relationship with El Niño is rather tenuous, although it is interesting to note that during the very strong El Niño of 1982/83 the oscillation was extremely weak.

As noted earlier, the projection of the IO on to the zonal mean u-wind ($\bar{u}$) appears to provide a useful measure of intraseasonal activity. In Fig. 14 the variance of the bandpass (20–100 day) filtered $\bar{u}$ from the JDP data has been plotted after applying a running mean of 100 days in length. This essentially shows how the intraseasonal activity is modulated at lower frequencies associated with seasonal and interannual time scales. Also shown in Fig. 14 are the SST anomalies for the Niño 3 (5°N–5°S, 90°W–150°W) region of the central and East Pacific. The preference for the IO to form during northern winter and spring is clearly evident. There is also a suggestion that the oscillation tends to be suppressed during the warm phase of El Niño, although the relationship is far from robust from such a limited sample and may depend on the phase of the El Niño with respect to the seasonal cycle.

When a similar diagnostic is computed for the three models with the strongest intraseasonal activity (UKMO, GLA, NCAR; see Table 2), there is little consensus on the seasonal and interannual variability of the intraseasonal activity (Fig. 15). During the very strong El Niño of 1982/83 all three models show reduced activity at intraseasonal time scales, in agreement with observations. However, for the rest of the AMIP decade, the influence of the SSTs seems to be minimal. For example, GLA has its strongest intraseasonal activity during the 1987 El Niño but weak activity during the 1982/83 El Niño.

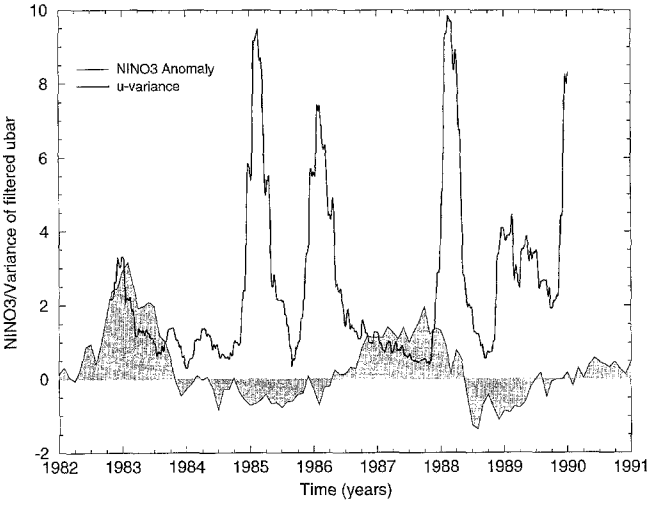

Fig. 14. Time series of the variance of the intraseasonal activity (20–100 days) in the zonal mean u-wind at 150 hPa from ECMWF analyses. A 100-day running mean has been applied to the variance time series. The *lower, shaded curve* is the sea surface temperature anomaly (K) for the NINO3 region

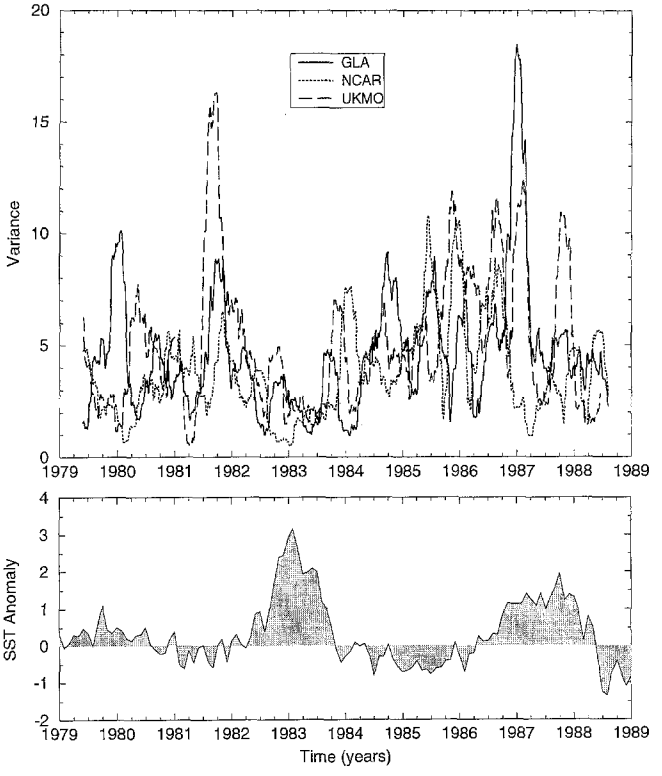

Fig. 15. Time series of the variance of the intraseasonal activity (20–100 days) in the zonal mean u-wind at 200 hPa for the three models (UKMO, GLA, NCAR) with the strongest intraseasonal activity. A 100-day running mean has been applied to the variance time series. The lower panel is the sea surface temperature anomaly (K) for the NINO3 region

5.4 *Relationship to characteristics of the basic climate*

The basic climate of each model has been studied using the monthly mean standard output available at PCMDI. A limited number of results will be presented

here based on the 9-year mean climate for December, January and February (DJF; 1979/80–1987/88). The fields chosen for presentation are the total precipitation (Fig. 16), the zonal cross-section of the mean meridional circulation (Fig. 20), and the 200 hPa zonal wind (Fig. 21). Verification for the precipitation is taken from the climatology derived from observations made by the microwave sounding unit (MSU, Spencer 1993) for the same period. No verification for the mean meridional circulation is shown since the various climatologies derived from NWP analyses depend on the characteristics of the forecast model. For the zonal wind field, the climatology from ECMWF analyses is shown for comparison.

As Fig. 16 demonstrates, the model simulations of precipitation can differ dramatically. Some models show a tendency to produce a split Inter-Tropical Convergence Zone (ITCZ) in the West Pacific which seems to be related to the use of moisture convergence closure in the convection scheme (e.g., BMRC, ECMWF). As Hess et al. (1993) noted in their study of the formation of ITCZs in an aquaplanet model, a Kuo-type convection scheme tends to produce a split ITCZ associated with the formation of mixed Rossby-gravity waves. However, the development of a split ITCZ may also be require the horizontal resolution to be sufficiently high (say T42) for these tropical synoptic systems to be resolved. Sumi (1992) found that a Kuo scheme used in an aquaplanet model at T21 resolution tended to produce a single ITCZ whereas the same model run at T42 resolution produced symmetric ITCZs located at about 10° latitude off the equator, similar to those noted by Hess et al. (1993).

It has long been recognized that convective activity over the tropical oceans is strongly correlated with SST (e.g., Riehl 1954), with convection most likely to occur for SSTs in excess of 28 °C (e.g., Webster and Lukas 1992). If the precipitation distribution from each model (Fig. 16) is compared with the mean SSTs for DJF (Fig. 17a), then it is clear that the relationship with SST is demonstrably weak in some models. The observed relationship between rainfall, as estimated from the microwave sounding unit (MSU, Spencer 1993), and SST during the AMIP decade is shown in Fig. 17b for the region 140°E–120°W, 20°S–0°, denoted by the box in Fig. 17a. A linear least-squared fit to the data indicates that, in this region, precipitation increases by 3.1 (mm/day)/°C. (Note: the dependence between the MSU rainfall estimates and the SST is not established a priori since the MSU channel 1 observes "the cloud water thermal emission, and to a lesser extent rainwater" and the retrieval formulation corrects for airmass temperature, Spencer 1993). Analysis of the precipitation/SST relation for each of the models indicates that there are substantial differences in the strength of their response to the imposed boundary forcing (Fig. 18). For example, models with the strongest IO (UKMO, GLA, NCAR, see Table 2) exhibit a dependence that is as strong as, or stronger than observed, while models with a weak IO (MRI, LMD, ECMWF) are much less sensitive to the SSTs. Also, the scatter of the model data suggests that the models generally exhibit greater variability than that in the MSU data, which is consistent with their lower rainfall/SST pattern correlations than observed ($r=0.87$). In the case of the models considered in Fig. 18, those with a strong IO have higher rainfall/SST pattern correlations ($r=0.73$ to 0.83) compared with the models that have a weak IO ($r=0.50$ to 0.62).

As a result of the variable sensitivity to SST exhibited by the models, the precipitation along the South Pacific Convergence Zone (SPCZ), an important climatological feature extending over the central Pacific and related to the warm SSTs, is not well represented in some of the models (Fig. 16). This may have implications for the development and maintenance of intraseasonal oscillations. If the intraseasonal oscillation is viewed as a moist Kelvin wave maintained by diabatic heating, then, in very simple terms, those models with reduced precipitation in the central Pacific will have conditions in which the wave is more quickly dissipated and thus less likely to maintain eastward propagation. This behavior is seen in idealized model studies (e.g., Bladé and Hartmann 1993) where a longitudinal variation in the heating intensity from marginally unstable to stable or neutral conditions gives rise to differing degrees of dissipation for the eastward propagating, equatorially trapped CISK/moist Kelvin wave mode.

It is interesting to note that those models with a reasonable simulation of intraseasonal activity (e.g., UKMO, GLA, NCAR) have extensive precipitation along the SPCZ. In contrast, those models with a poor simulation of the SPCZ (e.g., ECMWF, MRI) have weaker intraseasonal behavior and less evidence of a coherent eastward propagating signal. The exception to this is the CSU model which has a reasonable simulation of the SPCZ but a very weak IO. If the longitudinal distribution of precipitation, averaged between the equator and 20°S, is plotted for three models with a weak IO (MRI, LMD, ECMWF) and for three models with a strong IO (UKMO, GLA, NCAR: Fig. 19), then there is an indication that a reasonable simulation of the IO is related to stronger heating in the West and Central Pacific. However, there is clearly no simple relationship between these two parameters since many other factors are likely to be involved. The results nevertheless suggest that the ability of a GCM to reproduce the observed correlation between convective activity and SST may be one prerequisite for giving a reasonable simulation of the intraseasonal oscillation.

As well as a wide range of patterns in the precipitation distributions shown in Fig. 16, the mean meridional circulation simulated by each model also suggests very differing representations of the vertical profiles of heating primarily associated with cumulus convection (Fig. 20). Studies of the intraseasonal oscillation using idealized models have shown that the phase speed may be dependent on the vertical scale of the heating (e.g., Lau et al. 1988) with the implication that lower phase speeds are associated with increased heating in the lower troposphere. In this study there does not appear

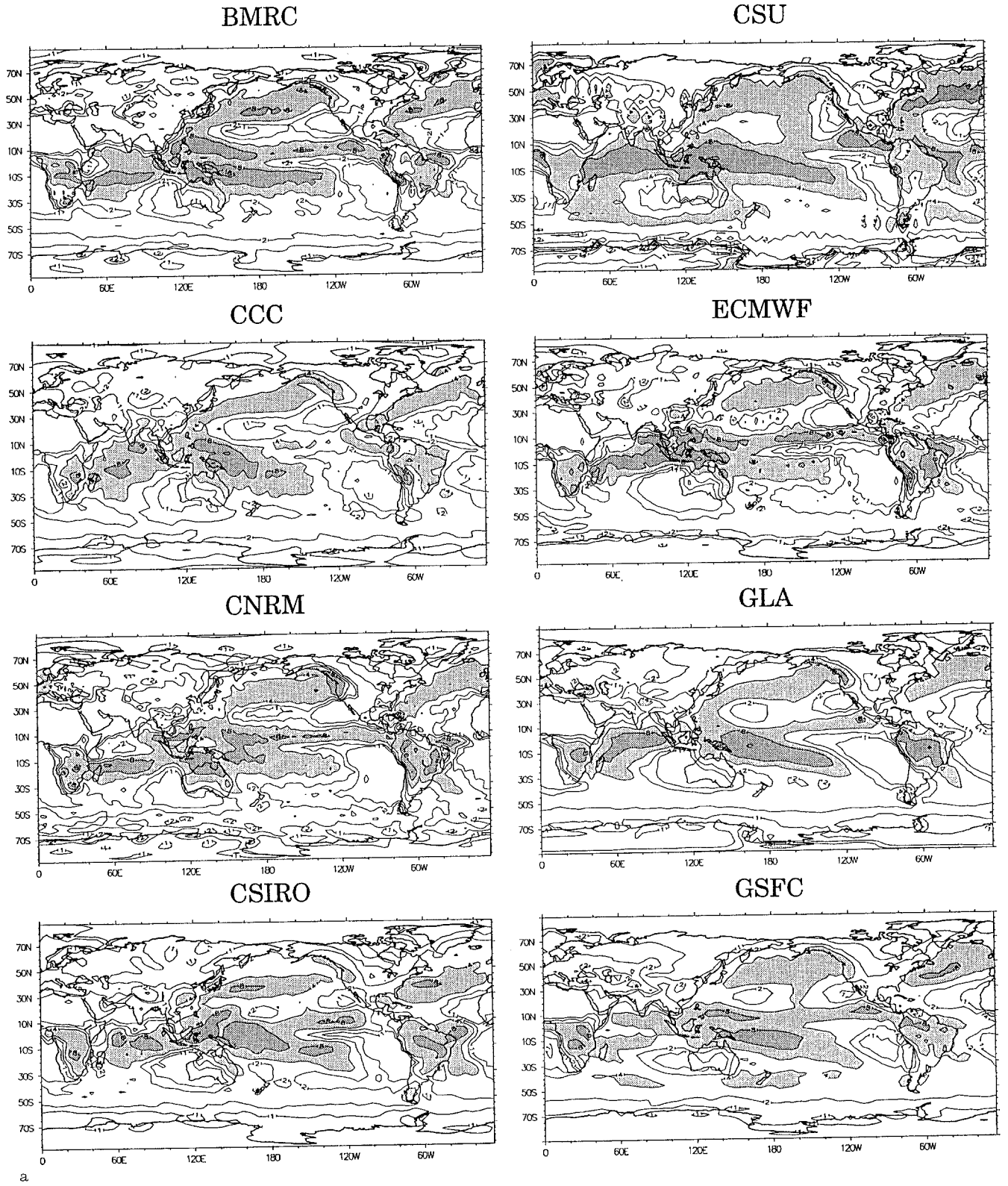

a

Fig. 16. 9-year mean (1979/80–1987/88) precipitation climatology for DJF from the participating models. Contours are drawn at 1, 2, 4, 8 and 16 mm/day and values in excess of 4 mm/day are *shaded*. The last panel is the mean precipitation climatology for DJF derived from the MSU observations for the same period

to be a consistent relationship between the phase speed of the simulated oscillations and the depth of the heating implied by the mean meridional circulation. However, as already noted, those models with strong, deep heating appear to give the most realistic oscillations in terms of amplitude and propagation characteristics. Consistent with the suggestion that a reasonable simulation of the SPCZ may be important, those mod-

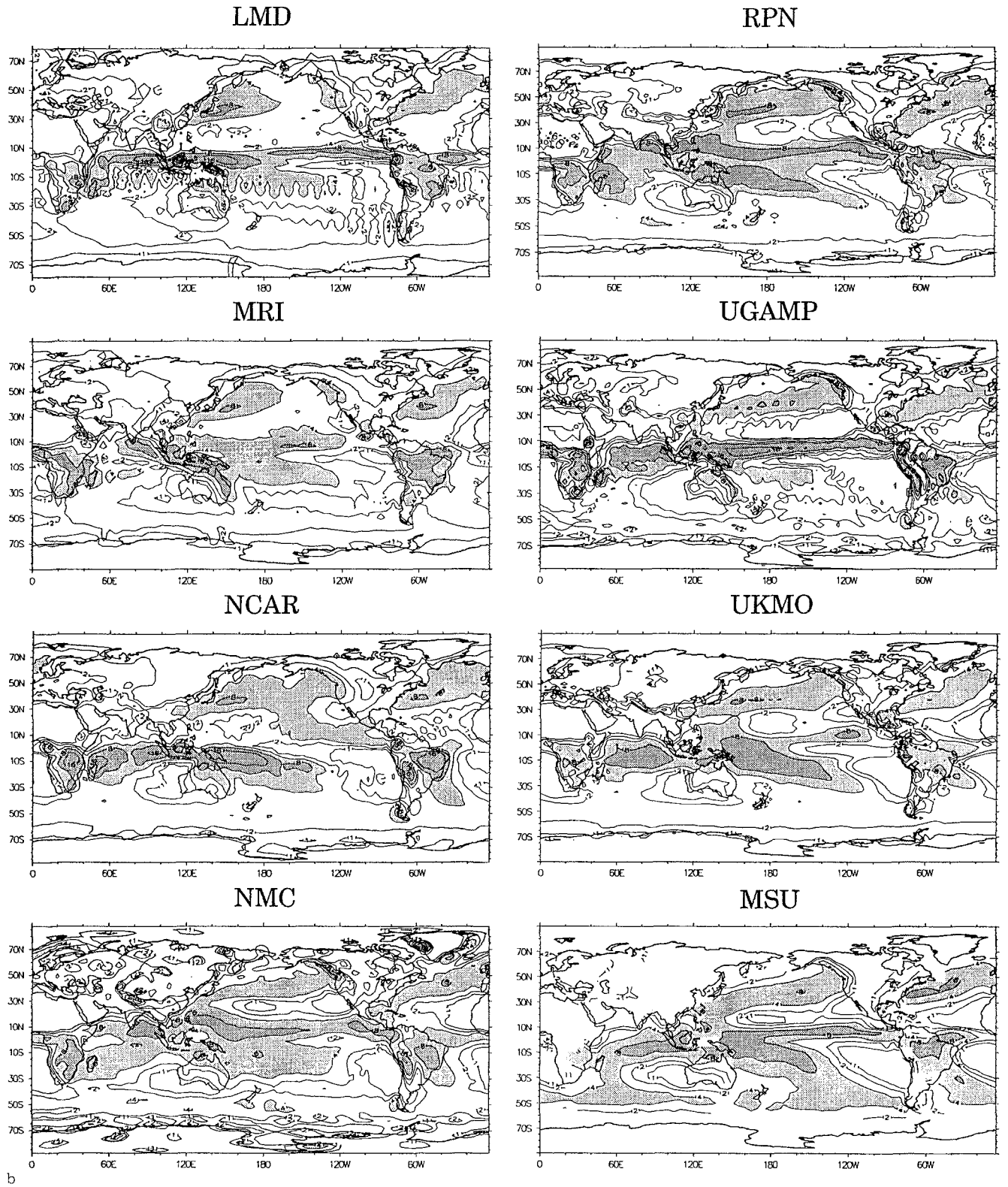

b

els with most skill at intraseasonal time scales tend to have the main ascending branch of the Hadley circulation located south of the equator.

The variation between the models in the depth of the diabatic heating, implied by the mean meridional circulation (Fig. 20), may have implications for the response of the upper tropospheric flow to perturbations in the diabatic heating associated with seasonal and intraseasonal time scales. GLA, NCAR and UKMO, which have high activity at these time scales, all simulate very strong, deep, time-mean Hadley circulations. Consistent with the arguments presented in Section 4, the 200 hPa zonal wind distributions (Fig. 21) show that these models also produce strong westerlies in the

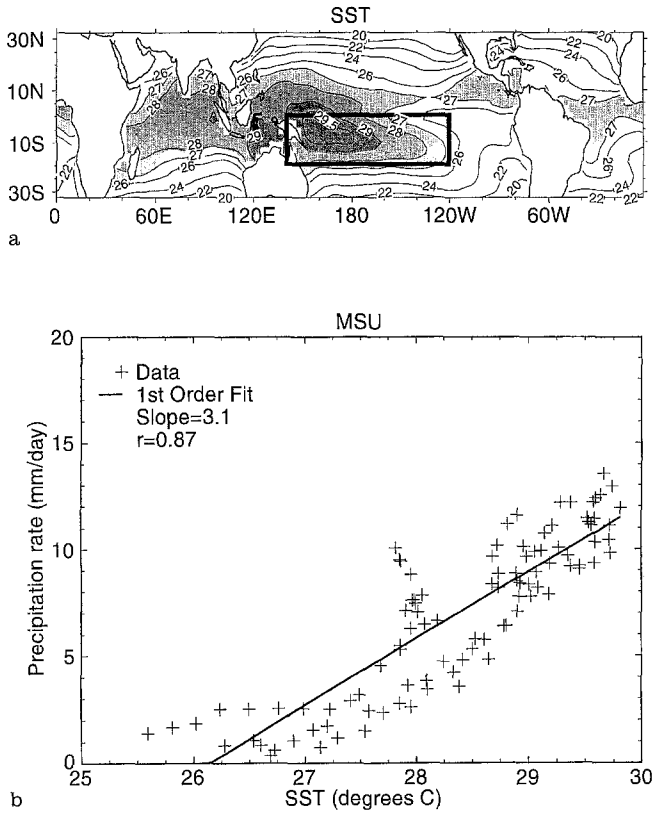

Fig. 17a, b. 9-year mean (1979/80–1987/88) sea surface temperature (°C) distribution for DJF from AMIP. Contours are drawn at 20, 22, 24, 26, 27, 28, 29 and 29.5 °C. Values in excess of 27 °C are *shaded*. **b** Scatter plot of the precipitation from the MSU observations versus the sea surface temperatures from the 9 year mean climatologies for DJF from the boxed region in **a**. The *solid line* represents the linear least squared fit. The slope of the linear fit and the pattern correlation coefficient (r) are given

equatorial central and East Pacific associated with both the divergent and rotational components of the flow. The simulation of these equatorial westerlies may have implications for interactions with the extratropics (Kiladis and Weickmann 1992), and thus may be important for the maintenance and eastwards propagation of the IO if it is viewed in terms of an interaction with the extratropics as proposed by Hsu et al. (1990). In contrast, the mean meridional circulation from the NMC model, for example, suggests that the vertical extent of the heating is not very deep or strong. The response of the upper tropospheric rotational flow is to produce weaker downstream twin cyclones over the central and East Pacific with consequently an easterly bias in the zonal wind in this region (Fig. 21).

A relationship between intraseasonal activity and the upper tropospheric zonal flow is unclear from these results. The importance of the longitudinal variation in the basic state with respect to the dynamical response to ENSO and to the intraseasonal oscillation was alluded to in Section 4 with regard to the seasonality of the response. The transition from upper level easterlies to westerlies across the equatorial Pacific implies a substantial longitudinal variation in the vertical wind shear, since the lower tropospheric flow is predominantly easterly. If the assumption is made that the IO consists of a Kelvin wave, modified by a forced Rossby wave, then, since the propagation of a Kelvin wave appears to be inhibited in regions of westerly shear (e.g., Lim et al. 1991), this might suggest that the IO would be less coherent in those models with strong longitudinal variation in the equatorial zonal wind. This does not seem to be the case from the results shown here. In fact, as already noted, a strong longitudinal variation in the zonal wind is a consequence of strong heating in the central and West Pacific which appears to be a necessary condition for producing intraseasonal variability of reasonable amplitude.

6 Discussion

This study has presented the results of the preliminary assessment of the intraseasonal oscillation simulated by 15 atmospheric GCMs as part of AMIP. The analysis has been necessarily limited by the availability of data, but nevertheless, the results suggest that not only is there a wide range of skill, but also that so far no model appears to simulate the dominant aspects of the observed intraseasonal oscillation. There is evidence of an eastward propagating, large-scale disturbance in a number of models and future analysis will concentrate on identifying the structures associated with it, probably through the use of EOF techniques.

Interactions between multiple time scales of variability in the tropics have been the subject of several papers (e.g., Nakazawa 1988; Lau et al. 1991), suggesting that the synoptic scale, higher frequency modes of convective activity are modulated by the intraseasonal oscillation. How much the synoptic and mesoscale activity embedded within the intraseasonal oscillation is responsible for the evolution of the oscillation itself remains an open question (e.g., Hendon and Liebmann 1994). This study has shown that although the majority of models underestimate the activity at intraseasonal time scales, those models which do have adequate power at these frequencies, appear, however, to overestimate the variance at higher frequencies. Thus the relationship between these time scales clearly needs to be understood. Once the full history data for OLR become available, a subsequent phase of this subproject will assess the organization of convection in GCMs at all time scales. Recently Takayabu (1994), using geostationary satellite data, has shown that large-scale features of cloud systems can be identified with particular equatorial waves. Whether such a relationship exists in a GCM and whether these waves are adequately represented needs to be assessed.

The results of this study suggest that the hierarchical structure of convective activity also extends to the longer time scales with an inferred relationship between intraseasonal activity and the strength of the seasonal cycle. This may be saying nothing more than that a particular model is more active at all time scales, but it does point to a possible basic requirement that a GCM should be able to represent the seasonal cycle

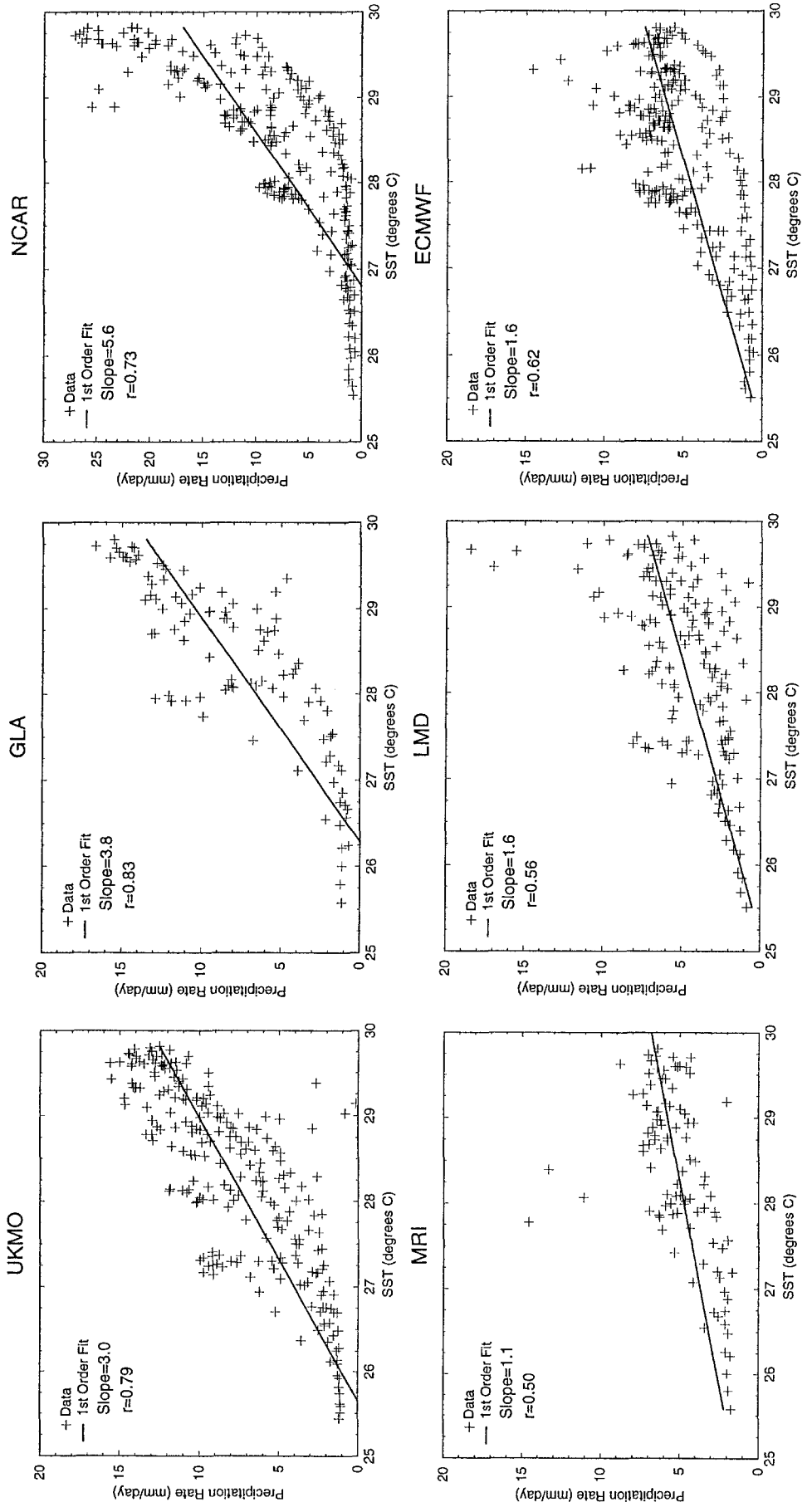

Fig. 18. As Fig. 17b, but for three models with strong, and three models with weak intraseasonal activity (note the y-axis scale change for the NCAR simulation)

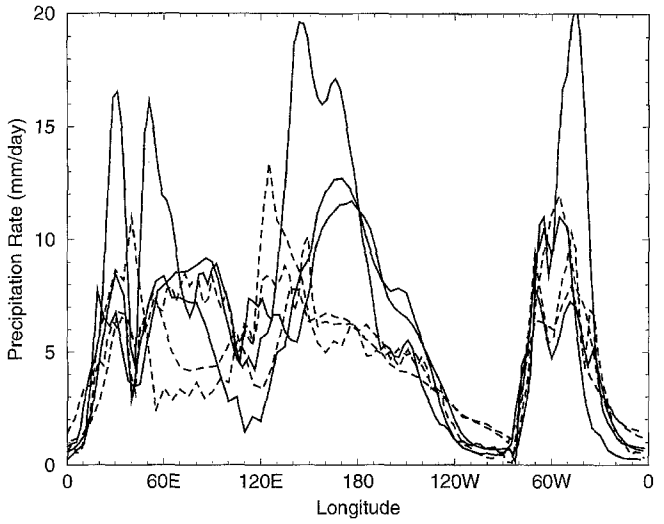

Fig. 19. Longitudinal distribution of precipitation (mm/day) averaged between 0° and 20°S from the 9-year mean DJF climatology for the three models with strong (*solid lines*), and the three models with weak (*dashed lines*) intraseasonal activity presented in Fig. 18

with some fidelity. The seasonal cycle involves changes in the heating pattern forced primarily by the solar seasonal cycle and continentality. However, since these changes in the heating distribution force the planetary scale waves and hence modulate the general circulation, as discussed in Section 4, it indicates how well the model is able to respond to a modulation of the heating pattern at other time scales.

The seasonality of the observed intraseasonal oscillation is pronounced, with its maximum activity near the vernal equinox, but yet no GCM was able to reproduce it adequately. This seasonality appears to be closely related to the semiannual migration of the climatological convection across the equator which is itself driven by the SSTs. As idealized modelling studies have shown (e.g., Salby et al. 1994), greatest amplification of the equatorial Kelvin wave and associated subtropical Rossby gyres occurs when the atmospheric heating is maximized at the equator. This occurs preferentially during the vernal equinox when the SST maximum is on the equator over the entire eastern hemisphere. In contrast, at the autumnal equinox the warmest SSTs in the Pacific still lie in the Northern Hemisphere, and the migration of the mean ITCZ southwards into the Southern Hemisphere does not occur until almost the end of the year. The fact that no GCM was able to simulate the correct seasonality of the IO corroborates the need for an accurate representation of the seasonal cycle.

From the limited sample provided by the JDP, there appears to be substantial interannual variability in the occurrence and strength of the IO. It is not clear how or whether this is related to ENSO, despite the suggestion from idealized models (e.g., Bladé and Hartmann 1993) that the longitudinal variation in SST may have a considerable impact on the development and propagation of an equatorial Kelvin wave. However, it is intriguing that in those models with strong intraseasonal activity, the oscillation appears to be suppressed during the intense El Niño of 1982/83. Analysis of extended GCM integrations with observed SSTs, covering several decades, may provide further clues, as may the reanalysis project in progress at NMC.

Although only a limited number of mean climatic fields have been studied, the general conclusion can be reached that a good simulation of the basic time mean climate is important for simulating the intraseasonal oscillation. A particular aspect that was noted was the correlation between tropical SST and convective activity. This basic relationship is not always well simulated, particularly in those models where the intraseasonal activity is weak. This link between SST and convection is important also in the evolution of the seasonal cycle, as discussed above, and may go some way to explaining both the apparent relationship between activity at seasonal and intraseasonal time scales (Fig. 12), and the problems with simulating the seasonality of the intraseasonal oscillation.

How well a model simulates the mean heating distribution also has implications for the circulation. Errors in the basic equatorial zonal flow may affect the propagation characteristics of equatorial waves. They may also influence the interaction between the extratropics and the tropics which may be important as a forcing mechanism for the intraseasonal oscillation (Hsu et al. 1990). Similarly the vertical profile of the heating may influence the basic flow through the strength of the forced Rossby waves, as discussed in Section 4, and may also affect the phase speed of the intraseasonal oscillation.

Certainly, other factors than those studied in this report may be relevant, but data availability has been a limiting factor. For example, idealized model studies (e.g., Salby et al. 1994) have suggested that static stability may play a key role in the IO since the Kelvin wave depends fundamentally on the Brunt-Väisälä frequency. If the static stability of the troposphere is increased then this opposes vertical motion and suppresses the feedback between the circulation and the convection so stabilizing the disturbance. The AMIP standard output does not have sufficient detail to determine the static stability over the equatorial oceans in the various models, although the zonal mean temperatures and humidities suggest a wide range of θ_e profiles when averaged between 10°N and 10°S (Fig. 22).

The dependence of intraseasonal activity on three basic aspects of a model's formulation (horizontal resolution, numerics, convective closure) have been summarized in Fig. 23. The distinction between 'high' and 'low' horizontal resolution has been based on whether a model would resolve a tropical synoptic scale system or not. Typically, T42 ($\sim 3°$ grid) would be sufficient, but not T21 ($\sim 5°$ grid). There are some concerns with spectral models about how the tendencies due to diabatic processes, which are computed in gridpoint space, project on to the dynamics, integrated in spectral space (Lander 1994). The models have also been classified in terms of the closure of the convection

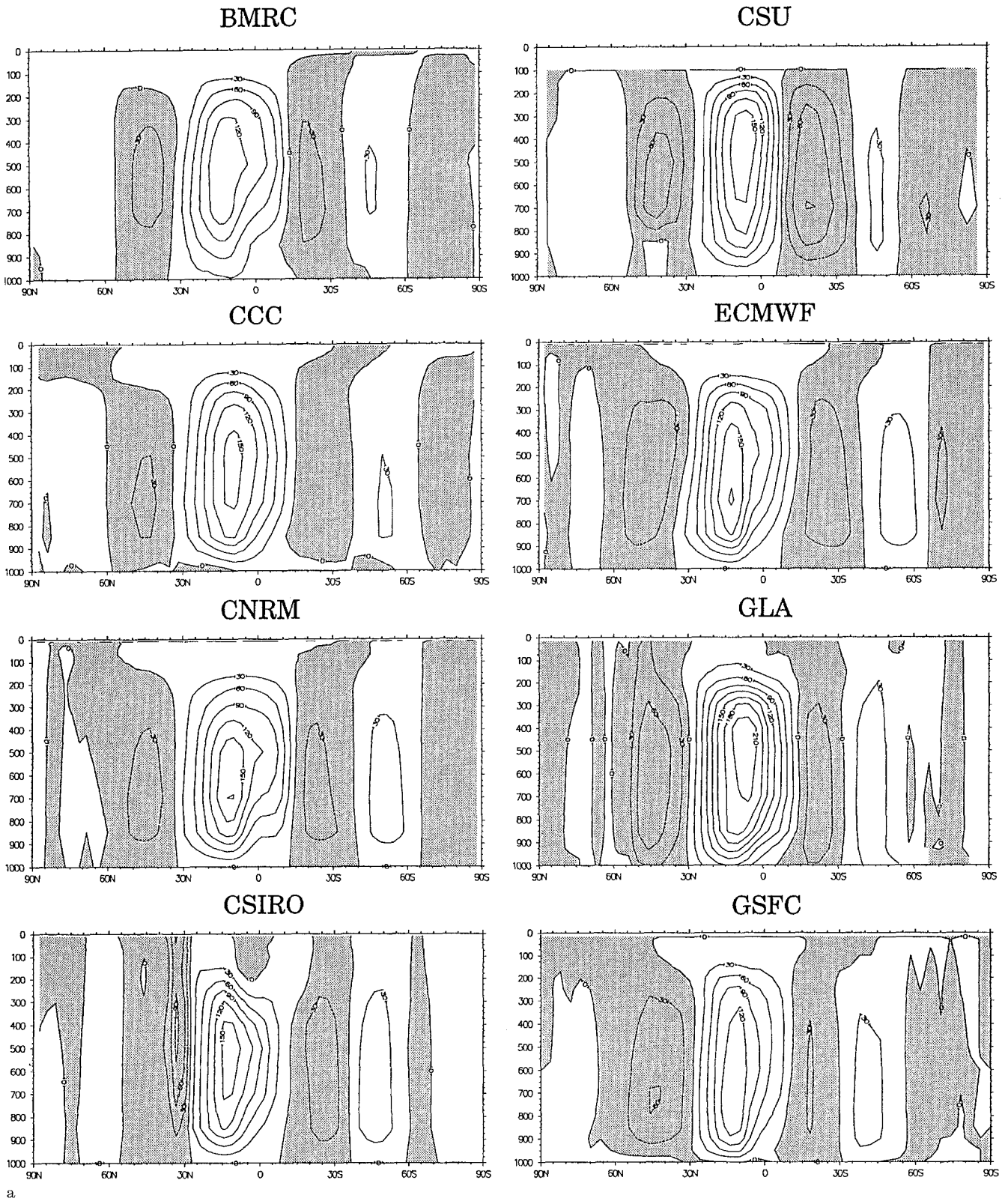

a

Fig. 20. As Fig. 16, but for the mean meridional circulation (10^9 kg s^{-1}). The contour interval is 30×10^9 kg s^{-1} and negative values are *shaded*

scheme. The sensitivity to the closure has been quantified in terms of the intraseasonal activity (Fig. 23c), and in terms of the relationship between precipitation and SST (Fig. 23d). In Fig. 23d, the slope of the linear fit between the precipitation and SST (Figs. 17 and 18) is used as a measure of the sensitivity of the convection to the SST.

The bar charts shown in Fig. 23 suggest that neither

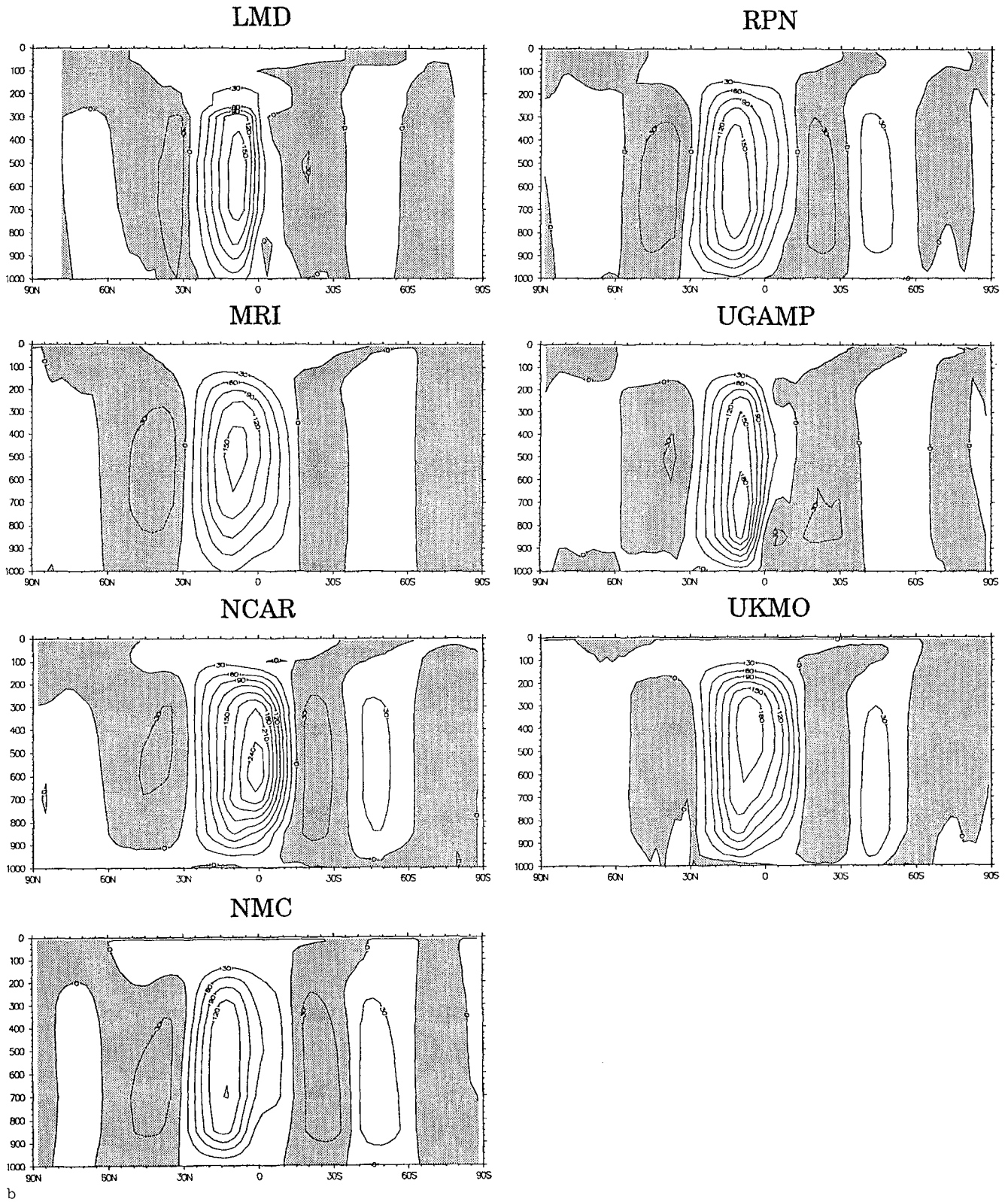

b

horizontal resolution nor numerics play an important role in determining a model's intraseasonal activity. However, the dependence of convective activity on moisture convergence does seem to be a factor. This result is consistent with the findings of Slingo et al. (1994), where they compared the transient activity produced by two very different convection schemes in the UGAMP GCM, and identified moisture convergence closure as being inappropriate. A recent study by Nordeng (personal communication), in which the moisture convergence dependence of the ECMWF convection scheme was replaced by a buoyancy criteri-

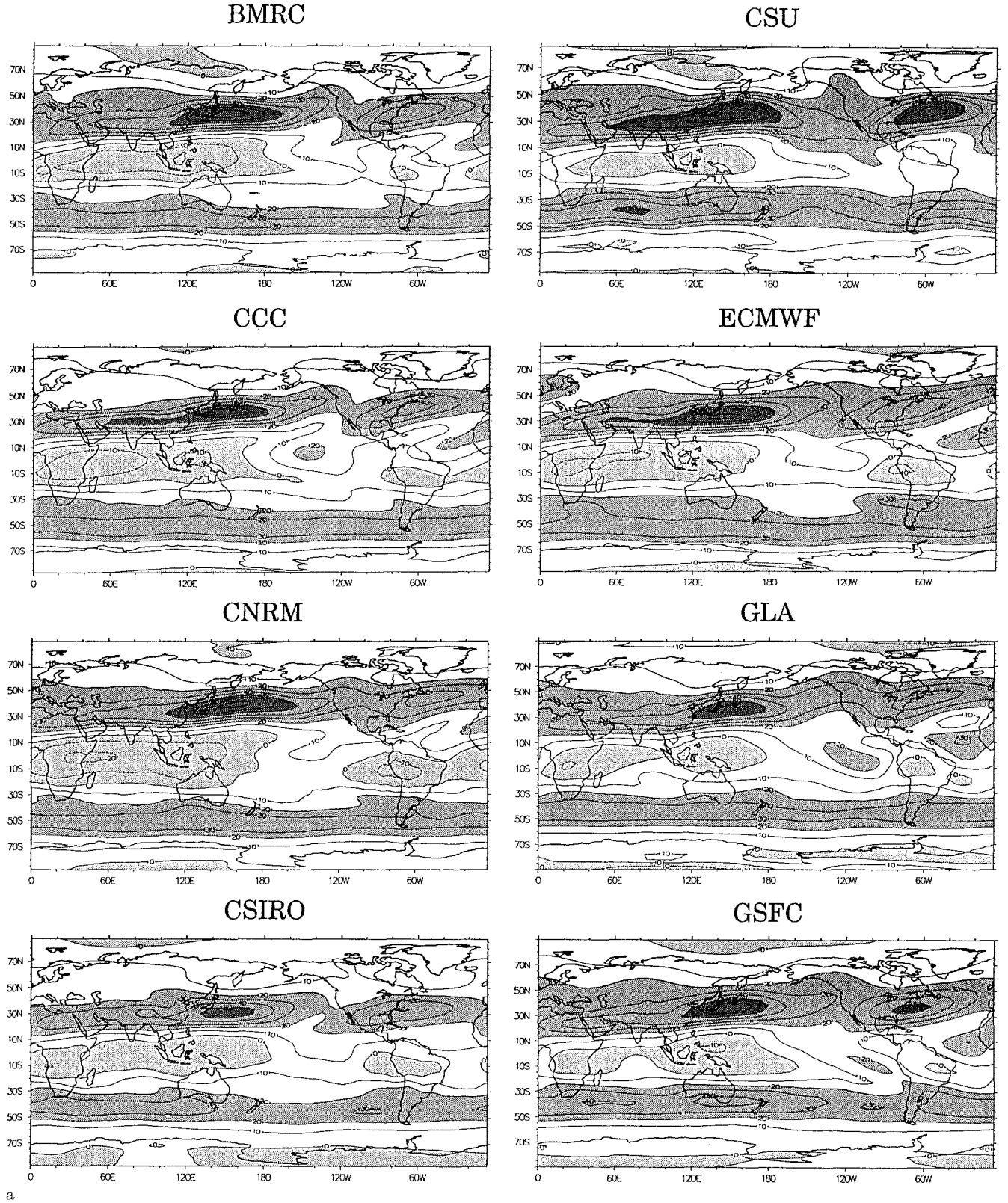

a

Fig. 21. As Fig. 16, but for the zonal wind at 200 hPa. The contour interval is 10 ms $^{-1}$. Easterlies, and westerlies in excess of 20 ms $^{-1}$, are *shaded*. The last panel is verification data from ECMWF/JDP analyses

on, showed a marked improvement (i.e., increase) in transient activity in the tropics of the ECMWF model. The results of this study (Fig. 23c) also suggest that those models with a reasonable level of intraseasonal activity have used convection schemes which are closed on buoyancy rather than moisture supply. In addition, the three models with the strongest IO not only have convection schemes which are closed on buoyancy,

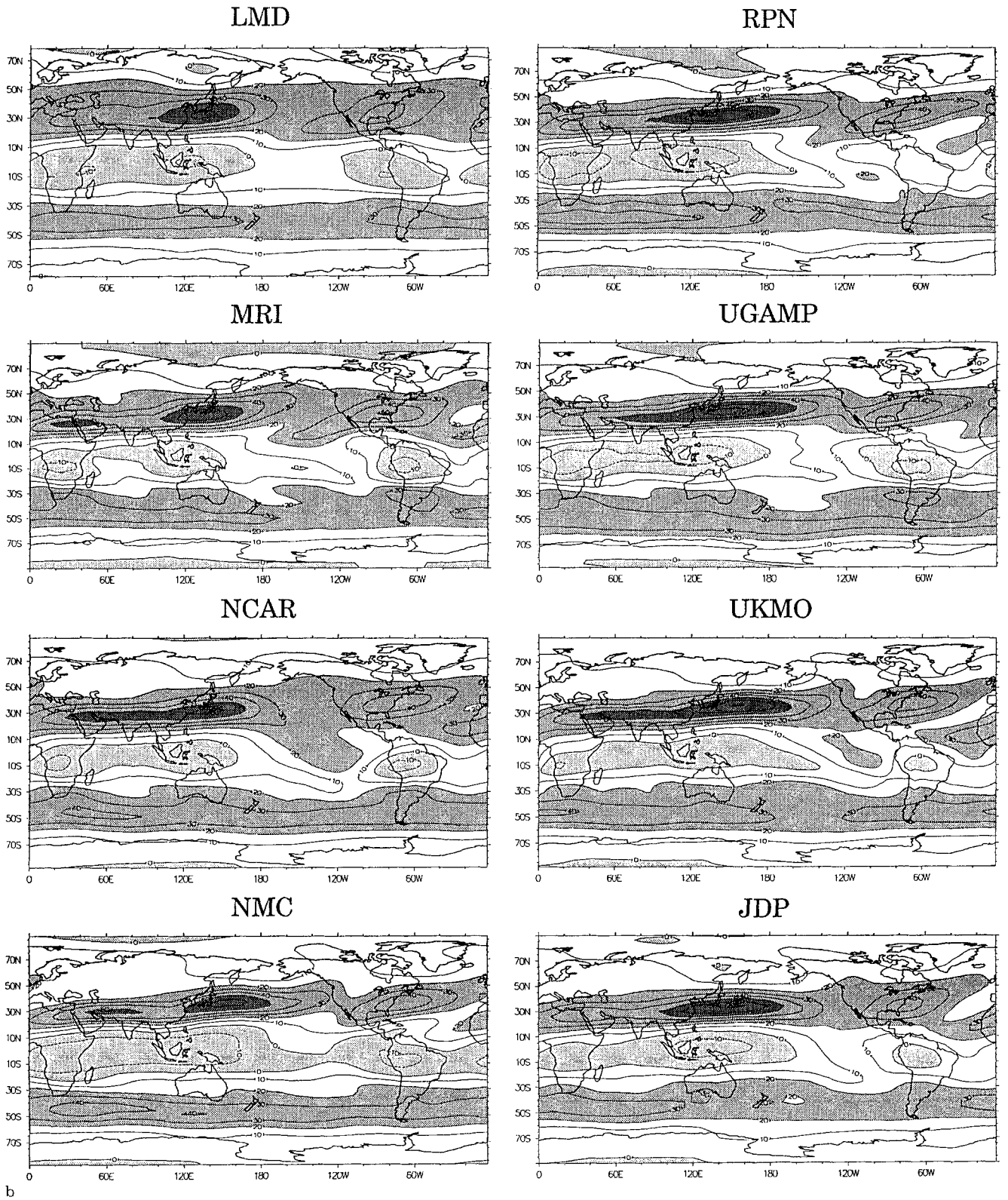

b

but, as Fig. 23d shows, are also the only models in which the relationship between precipitation and SST is as strong, or stronger than that inferred from the MSU precipitation climatology (Fig. 17b).

Although the results shown in Fig. 23 do not suggest any particular dependence on horizontal resolution, additional diagnosis from an ensemble of AMIP integrations made with the CNRM Arpège model suggest that there may be a high degree of sensitivity. Figure 24 shows the space time spectra for the wave-number 1 component of the 200 hPa velocity potential for each of the three resolution simulations (T21, T42 and T79). The spectra change substantially with an increase in resolution from T21 to T42, with a marked reduction in

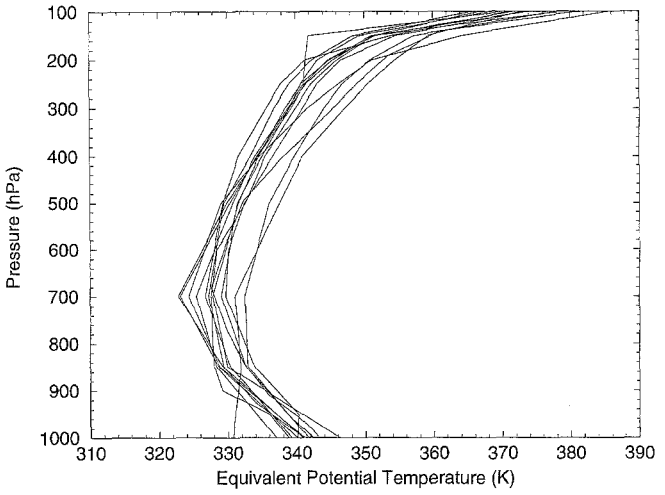

Fig. 22. Vertical profiles of the zonal mean equivalent potential temperature (θ_e) averaged between 10°N and 10°S from the DJF climatology for the participating models

power at all frequencies. The model has some peaks in activity at intraseasonal time scales with periods between 20 and 30 days when run at T21, but these are lost at higher resolutions. Whether other models show such a sensitivity to resolution is an interesting question.

Whilst the above analysis has concentrated on only three aspects of a model's formulation, other factors are undoubtedly important but may be difficult to quantify. Idealized model studies may well play a crucial role here by providing important clues concerning processes which may be influential in the simulation of the intraseasonal oscillation. For example, a recent study by Salby et al. (1994) has suggested that the oscillation may be very sensitive to boundary layer friction. They suggest that the sympathetic interaction between the convection and the large scale circulation, through the process termed 'frictional wave-CISK', can explain many aspects of the observed behavior of the IO in the eastern hemisphere. Due to frictional effects

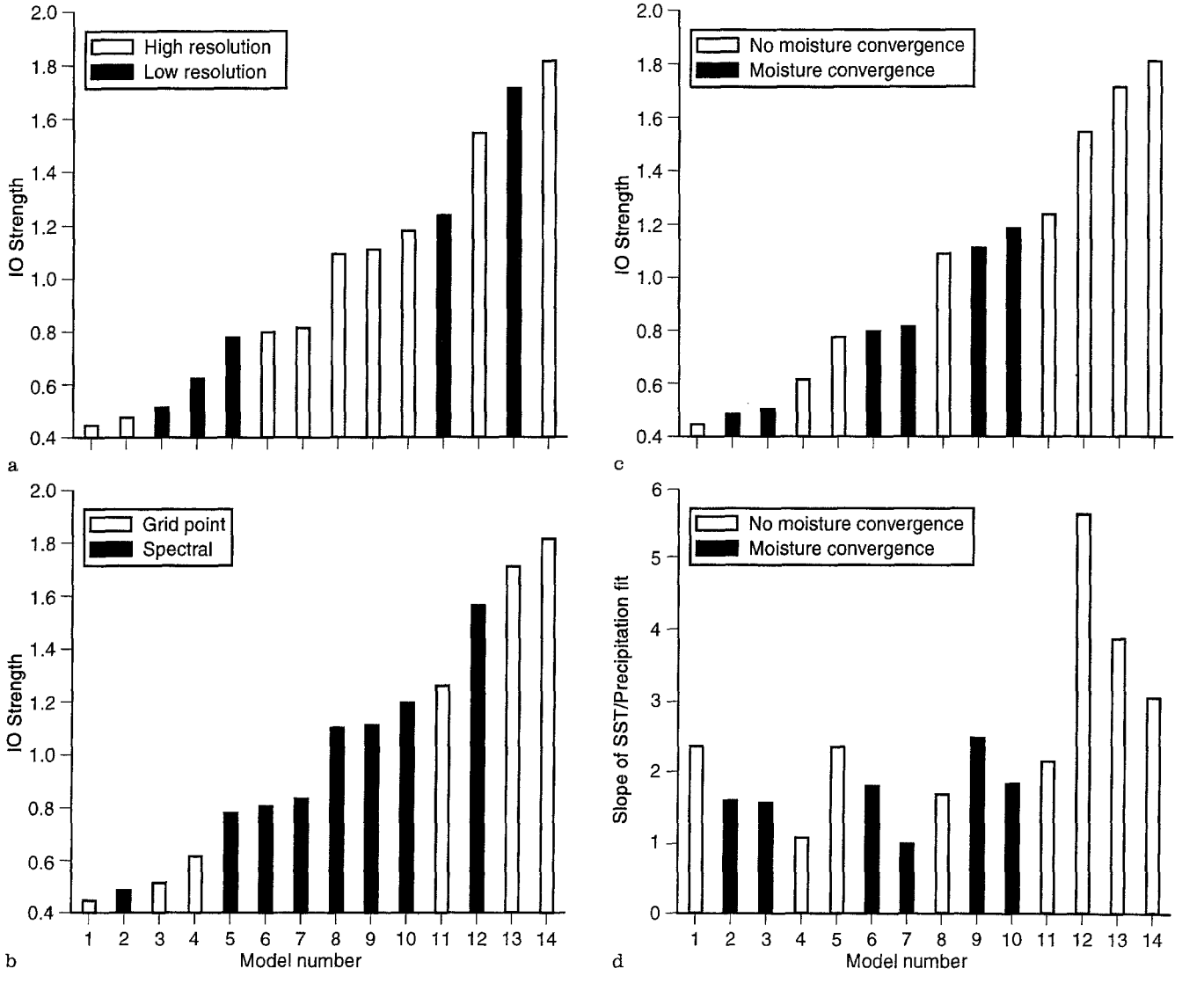

Fig. 23a–d. Bar charts showing the dependence of the participating models' intraseasonal activity on **a** horizontal resolution, **b** numerics and **c** convective parameterization closure. **d** shows the dependence of the slope of the precipitation/SST relationship (as shown in Fig. 18) on convective parameterization closure. The *model number* refers to those given in Table 2

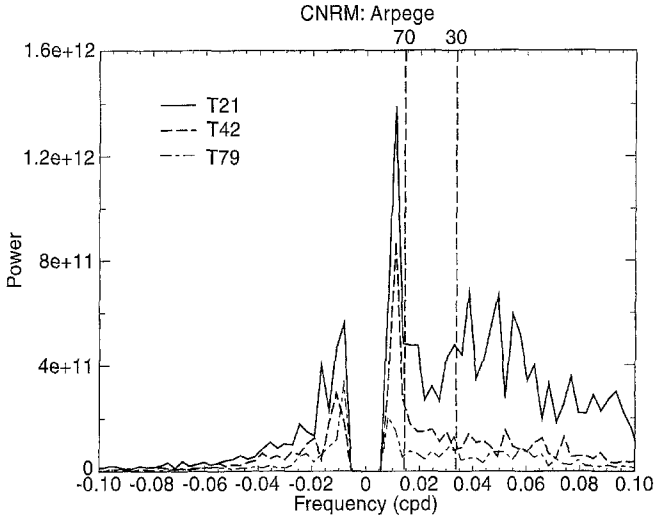

Fig. 24. Space-time spectra for the eastward and westward moving waves of the wave-number 1 seasonally detrended velocity potential from the CNRM Arpège model integrated at horizontal resolutions of T21, T42 and T79. The *dashed vertical lines* indicate periodicities of 70 and 30 days for eastward propagation

the surface convergence is shifted some 40–50° to the east of the heating, towards low pressure and in phase with the temperature anomaly associated with the Kelvin wave. Salby et al. (1994) also emphasize the importance of the Rossby gyres generated by the heating. In the amplifying phase of the IO their position is such as to reinforce the moisture convergence to the east of the heating, so providing the necessary conditions for the heating to amplify and propagate eastwards. The solutions described by Salby et al. (1994) are very sensitive to the boundary layer friction and suggest a possible area of research with a full GCM.

The structures in the moisture convergence field described by Salby et al. (1994) are quite meridionally confined and they question whether a low resolution GCM would be able to resolve them adequately. The results of this study do not, at present, support this, but because other factors are involved it may be difficult to disentangle the dependence on resolution. A later phase of the subproject, in which the structures associated with the simulated IO will be examined, will investigate whether frictional wave-CISK is a possible mechanism operating in the GCMs.

Idealized models may be able to explain many aspects of the IO in its convectively active phase over the eastern hemisphere, but they do not explain its behavior over the western hemisphere, nor how the oscillation is generated or amplified again over the Indian Ocean. The sporadic occurrence of the observed IO is an intriguing aspect of its behavior which might be due to stochastic forcing from the extratropics. The importance of the extratropics in forcing tropical convection, particularly during northern winter and spring, is apparent from satellite observations. The ability of GCMs to represent this interaction will form part of the later phases of this subproject.

7 Conclusions

An analysis of the ability of 15 atmospheric GCMs to simulate the tropical intraseasonal oscillation has shown that a wide range of skill exists. No model has successfully captured the dominance of the intraseasonal oscillation in the observations. The results suggest that an accurate simulation of the intraseasonal oscillation may be a demanding test of a GCM, because it has so many requirements. These may include good simulations of the basic climate, the seasonal cycle, higher frequency modes of tropical variability, and interactions with the extratropics. With regard to the basic climate, the results of this study suggest that an important aspect may be the relationship between convective activity and SST.

Acknowledgement. This work was performed under the auspices of the U.S. Department of Energy Environmental Sciences Division at the Lawrence Livermore National Laboratory under contract W-7405-ENG-48. Code for the computation of the filter weights was supplied by Dr. Mike Pedder (Reading University).

References

Bladé I, Hartmann DL (1993) Tropical intraseasonal oscillations in a simple nonlinear model. J Atmos Sci 50:2922–2939

Ferranti L, Palmer TN, Molteni F, Klinker E (1990) Tropical-extratropical interaction associated with the 30–60 day oscillation and its impact on medium and extended range prediction. J Atmos Sci 47:2177–2199

Gates WL (1992) AMIP: The Atmospheric Model Intercomparison Project. Bull Am Meteorol Soc 73:1962–1970

Gray BM (1988) Seasonal frequency variations in the 40–50 day oscillation. Int J Climatol 8:511–519

Hayashi Y (1982) Space-time spectral analysis and its application to atmospheric waves. J Meteorol Soc Japan 60:156–171

Hayashi Y, Golder DG (1993) Tropical 40–50- and 25–30-day oscillations appearing in realistic and idealized GFDL climate models and the ECMWF dataset. J Atmos Sci 50:464–494

Hendon HH, Liebmann B (1994) Organization of convection within the Madden-Julian oscillation. J Geophys Res 99:8073–8083

Hendon HH, Salby ML (1994) The life cycle of the Madden-Julian oscillation. J Atmos Sci 51:2225–2237

Hess PG, Battisti DS, Rasch PJ (1993) The maintenance of the intertropical convergence zones and the large-scale tropical circulation on a water-covered earth. J Atmos Sci 50:691–713

Hoskins BJ, Hsu HH, James IN, Masutani M, Sardeshmukh PD, White GH (1989) Diagnostics of the global atmospheric circulation based on ECMWF analyses 1979–1989 WCRP-27. World Meteorological Organization, Geneva

Hsu H, Hoskins BJ, Jin F (1990) The 1985/86 intraseasonal oscillation and the role of the extratropics. J Atmos Sci 47:823–839

Kiladis GN, Weickmann KM (1992) Circulation anomalies associated with tropical convection during northern winter. Mon Weather Rev 120:1900–1923

Knutson TR, Weickmann KM (1987) 30–60 day atmospheric oscillations: composite life cycles of convection and circulation anomalies. Mon Weather Rev 115:1407–1436

Kuhnel I (1989) Spatial and temporal variation in Australia-Indonesia region cloudiness. Int J Climatol 9:395–405

Lander J (1994) The interaction of numerics and physics in a spectral transform GCM. PhD Thesis, Department of Meteorology, Reading University, Reading, UK

Lau K-M, Chan PH (1985) Aspects of the 40–50 day oscillation during the northern winter as inferred from outgoing longwave radiation. Mon Weather Rev 113:1889–1909

Lau K-M, Chan PH (1988) Interannual and intraseasonal variations of tropical convection: a possible link between the 40–50 day oscillation and ENSO? J Atmos Sci 44:506–521

Lau K-M, Held IM, Neelin JD (1988) The Madden-Julian oscillation in an idealized general circulation model. J Atmos Sci 45:3810–3832

Lau K-M, Peng L, Sui CH, Nakazawa T (1989) Dynamics of super cloud clusters, westerly wind bursts, 30–60 day oscillations and ENSO: a unified view. J Meteorol Soc Japan 67:205–219

Lau K-M, Nakazawa T, Sui CH (1991) Observations of cloud cluster hierarchies over the tropical western Pacific. J Geophys Res 96:3197–3208

Lim H, Chang C-P, Lim T-K (1991) Vertical wind shear effects on Kelvin wave-CISK modes: possible relevance to 30–60 day oscillations. Terrest Atmos Oceanic Sci 2:203–216

Madden RA, Julian PR (1972) Description of global scale circulation cells in the tropics with 40–50 day period. J Atmos Sci 29:1109–1123

Madden RA, Julian PR (1994) Observations of the 40–50-day tropical oscillation – a review. Mon Weather Rev 122:814–837

Magaña V (1993) The 40- and 50-day oscillations in atmospheric angular momentum at various latitudes. J Geophys Res 98:10441–10450

Matthews AJ (1994) The intraseasonal oscillation. PhD Thesis, Department of Meteorology, University of Reading, Reading, UK

Murakami T, Chen L-X, Xie A, Shrestha ML (1986) Eastward propagation of 30–60 day perturbations as revealed from outgoing longwave radiation data. J Atmos Sci 43:961–971

Nakazawa T (1988) Tropical super clusters within intraseasonal variations over the western Pacific. J Meteorol Soc Japan 66:823–839

Park C-K, Straus DM, Lau K-M (1990) An evaluation of the structure of tropical intraseasonal oscillations in three general circulation models. J Meteorol Soc Japan 68:403–417

Phillips TJ (1994) A summary documentation of the AMIP models. PCMDI Rep 18, PCMDI, Lawrence Livermore National Laboratory, California

Rasmusson EM, Mo K (1993) Linkages between 200-mb tropical and extratropical circulation anomalies during the 1986–89 ENSO cycle. J Clim 6:595–616

Riehl H (1954) Tropical meteorology. McGraw-Hill, New York

Rosen RD, Salstein DA (1983) Variations in atmospheric angular momentum on global and regional scales and the length of day. J Geophys Res 88:5451–5470

Rui H, Wang B (1990) Development characteristics and dynamic structure of tropical intraseasonal convection anomalies. J Atmos Sci 47:357–379

Salby ML, Hendon HH (1994) Intraseasonal behavior of clouds, temperature and motion in the tropics. J Atmos Sci 51:2207–2224

Salby ML, Garcia RR, Hendon HH (1994) Planetary-scale circulations in the presence of climatological and wave-induced heating. J Atmos Sci 51:2344–2367

Sardeshmukh PD, Hoskins BJ (1988) The generation of global rotational flow by steady idealized tropical convergence. J Atmos Sci 45:1228–1251

Slingo JM, Madden RA (1991) Characteristics of the tropical intraseasonal oscillation in the NCAR Community Climate Model. QJR Meteorol Soc 117:1129–1169

Slingo JM, Sperber KR, Morcrette J-J, Potter GL (1992) Analysis of the temporal behavior of convection in the tropics of the ECMWF model. J Geophys Res 97:18119–18135

Slingo JM, Blackburn M, Betts A, Brugge R, Hoskins BJ, Miller MJ, Steenman-Clark L, Thuburn J (1994) Mean climate and transience in the tropics of the UGAMP GCM: sensitivity to convective parameterization. QJR Meteorol Soc 120:881–922

Slingo JM, Sperber KR, Boyle JS, Ceron J-P, Dix M, Dugas B, Ebisuzaki W, Fyfe J, Gregory D, Gueremy J-F, Hack J, Harzallah A, Inness P, Kitoh A, Lau WK-M, McAvaney B, Madden R, Matthews A, Palmer TN, Park C-K, Randall D, Renno N (1995) Intraseasonal oscillations in 15 atmospheric general circulation models (results from an AMIP Diagnostic Subproject). WCRP-88, WMO/TD-No. 661, WMO, Geneva

Spencer RW (1993) Global oceanic precipitation from the MSU during 1979–91 and comparison to other climatologies. J Clim 6:1301–1326

Sumi A (1992) Pattern formation of convective activity over the Aqua Planet with globally uniform sea surface temperature. J Meteorol Soc Japan 70:855–876

Takayabu YN (1994) Large scale cloud disturbances associated with equatorial waves. Part I: spectral features of the cloud disturbances. J Meteorol Soc Japan 72:433–450

Webster P, Lukas R (1992) TOGA COARE: The coupled ocean-atmosphere response experiment. Bull Am Meteorol Soc 73:1377–1416

Weickmann KM, Khalsa SJS (1990) The shift of convection from the Indian Ocean to the western Pacific Ocean during a 30–60 day oscillation. Mon Weather Rev 118:964–978